Spatial deformation in a Bayesian spatiotemporal model for incomplete matrix-variate responses

Rodrigo de Souza Bulhões^{1*}, Marina Silva Paez² and Dani Gamerman²

^{1*}Department of Statistics, Institute of Mathematics and Statistics, Federal University of Bahia, Av. Milton Santos, s/n, Salvador, 40.170-110, Bahia, Brazil.

²Department of Statistical Methods, Institute of Mathematics, Federal University of Rio de Janeiro, Av. Athos da Silveira Ramos, 149, Rio de Janeiro, 21.941-909, Rio de Janeiro, Brazil.

*Corresponding author(s). E-mail(s): rbulhoes@ufba.br; Contributing authors: marina@im.ufrj.br; dani@im.ufrj.br;

Abstract

In this paper, we propose a flexible matrix-variate spatiotemporal model for analyzing multiple response variables observed at spatially distributed locations over time. Our approach relaxes the restrictive assumption of spatial isotropy, which is often unrealistic in environmental and ecological processes. We adopt a deformation-based method that allows the covariance structure to adapt to directional patterns and nonstationary behavior in space. Temporal dynamics are incorporated through dynamic linear models within a fully Bayesian framework, ensuring coherent uncertainty propagation and efficient state-space inference. Additionally, we introduce a strategy for handling missing observations across different variables, preserving the joint data structure without discarding entire time points or stations. Through a simulation study and an application to real-world air quality monitoring data, we demonstrate that incorporating spatial deformation substantially improves interpolation accuracy in anisotropic scenarios while maintaining competitive performance under near-isotropy. The proposed methodology provides a general and computationally tractable framework for multivariate spatiotemporal modeling with incomplete data.

Keywords: Multivariate space-time analysis, anisotropy, nonstationary spatial covariance modeling, geostatistics, dynamic linear models, missing observations

1 Introduction

Environmental data sets are typically characterized by processes observed over a finite set of times at fixed monitoring sites within a geographic region. Over the past decades, several spatiotemporal models have been developed to analyze such processes. These models often assume that the process of interest follows a Gaussian process with a mean function and a valid covariance structure given by the product of a variance parameter and an isotropic correlation function, defined in terms of the Euclidean distance between locations (Schmidt and Guttorp 2020). As noted by Guttorp and Schmidt (2013), this implies translation and rotational invariance of the process—properties that characterize isotropy and stationarity, often referred to as spatial homogeneity.

However, the assumption of isotropy is frequently unrealistic for many environmental variables such as temperature, pollution, soil moisture, or rainfall. These processes are influenced by local factors that induce directional dependence or spatial heterogeneity, including landscape, topography, prevailing winds, and proximity to the ocean (Morales et al. 2013, 2022). To address such nonstationary behavior, several methods have been proposed, the most common being the deformation approach, convolution-based methods, inclusion of covariates in the covariance function, and the stochastic partial differential equation (SPDE) approach (Mardia and Goodall 1993; Sampson et al. 2001; Sampson 2010; Guttorp and Schmidt 2013; Schmidt and Guttorp 2020).

Among these, the deformation approach introduced by Sampson and Guttorp (1992) has become a key framework for modeling non-homogeneous spatial processes. The core idea is to map the original geographic coordinates into a latent space where isotropy holds, typically using multidimensional scaling for the latent coordinates and thin-plate splines for interpolation at ungauged sites. In their formulation, temporal stationarity is assumed, with temporal dependence handled by detrending and analyzing the residuals as repeated measurements. Later Bayesian formulations (Damian et al. 2001; Schmidt and O'Hagan 2003) incorporated uncertainty in the latent coordinates, and subsequent works (Damian et al. 2003; Bruno et al. 2009) relaxed the assumption of temporal stationarity by including temporal trends. However, in these latter approaches, parameter estimation was generally performed in separate stages.

Under the assumption of isotropy, Bayesian dynamic models (West and Harrison 1997) have also been applied to spatiotemporal data (Sansó and Guenni 1999; Stroud et al. 2001; Huerta et al. 2004). These models not only relax temporal stationarity but also provide a unified framework for quantifying uncertainty and incorporating explanatory variables. Schmidt et al. (2011, Sec. 3) and Morales et al. (2013) employed Bayesian dynamic models to handle temporal variation and suggested correcting anisotropy via spatial deformation, allowing simultaneous estimation of spatial and temporal components within a single inferential step.

In this manuscript, we aim to analyze multidimensional spatiotemporal processes observed over a finite set of times at fixed monitoring stations. Building upon the matrix-normal Bayesian dynamic framework (Quintana 1987; Landim and Gamerman 2000), Paez et al. (2008) proposed modeling matrix-variate data using an isotropic Matérn covariance function to describe spatial dependence. Their results demonstrated

that joint modeling of multiple response variables substantially improves interpolation accuracy compared with univariate approaches.

Here, we extend the matrix-normal Bayesian dynamic model of Paez et al. (2008) to incorporate anisotropy through spatial deformation, allowing spatial dependence to be represented in a deformed latent space while preserving the temporal dynamics through the Bayesian state-space formulation. To perform inference, we develop an efficient Markov chain Monte Carlo algorithm for sampling from the posterior distribution of the model parameters.

The remainder of this paper is organized as follows. Section 2 presents the proposed spatiotemporal model for complete matrices. Section 3 extends the model to accommodate incomplete matrices and describes the imputation of missing values. Section 4 discusses the interpolation problem. Section 5 presents criteria for model comparison. A simulation study and an application are provided in Sections 6 and 7, respectively. Finally, Section 8 offers concluding remarks.

2 Spatiotemporal model for matrix-variate responses

2.1 General framework

We are interested in modeling multivariate spatiotemporal processes observed at a finite number of monitoring sites and time points. At each time t and location \underline{s} , a q-dimensional response vector $Y(\underline{s},t) = (Y_1(\underline{s},t),\ldots,Y_q(\underline{s},t))$ is recorded, representing multiple environmental variables measured simultaneously over space and time.

Formally, let $S \subset \mathbb{R}^2$ denote the spatial domain of interest and $\mathcal{T} = \{1, \ldots, T\}$ the discrete time index. The process $\{Y(\mathbf{s},t) : \mathbf{s} \in S, t \in \mathcal{T}\}$ is assumed Gaussian. Observations are available at N fixed sites $\mathbf{s}_1, \ldots, \mathbf{s}_N$, with coordinates $\mathbf{s}_n = (\text{lon}_n, \text{lat}_n)$ for $n \in \{1, \ldots, N\}$. The notation $Y_{n,i,t} = Y_i(\mathbf{s}_n, t)$ refers to the value of the ith response at site \mathbf{s}_n and time t, with $i \in \{1, \ldots, q\}$. For each $t \in \mathcal{T}$, the $N \times q$ response matrix is

$$\mathbf{Y}_{t} = \begin{bmatrix} Y_{1,1,t} & \cdots & Y_{1,q,t} \\ \vdots & \ddots & \vdots \\ Y_{N,1,t} & \cdots & Y_{N,q,t} \end{bmatrix}, \tag{1}$$

whose *i*th column $\mathbf{Y}_{i,t} = \begin{bmatrix} Y_{1,i,t} & \cdots & Y_{N,i,t} \end{bmatrix}^{\top}$ collects all N spatial observations of variable i at time t.

This matrix representation allows the model to capture both (i) dependence over time, through the evolution of regression parameters, and (ii) dependence across space, through a covariance structure that accounts for anisotropy and deformation.

2.2 Modeling spatial dependence through deformation

Spatial correlation is rarely isotropic in environmental data. To flexibly describe anisotropy, we adopt the deformation approach of Sampson and Guttorp (1992), in which the observed geographic coordinates are mapped to a latent space $\mathcal{D} \subset \mathbb{R}^2$ where isotropy approximately holds.

Let $d(\cdot)$ denote this mapping, with $d(\mathbf{g}_n) = \mathbf{d}_n = \begin{bmatrix} d_1(\mathbf{g}_n) & d_2(\mathbf{g}_n) \end{bmatrix}^{\top}$ and collect the latent coordinates in the $2 \times N$ matrix $\mathbf{D} = \begin{bmatrix} \mathbf{d}_1 & \cdots & \mathbf{d}_N \end{bmatrix}$. In the deformed space, we specify the spatial correlation between process values (or, equivalently, between location-indexed random components in the hierarchy) at sites \mathbf{g}_n and $\mathbf{g}_{n'}$ as a function of the Euclidean distance between their deformed coordinates. Concretely, the $N \times N$ matrix \mathbf{B} that governs spatial dependence across locations in the likelihood term has entries

$$B_{n,n'} = \rho_{\phi}(\|d(\mathbf{\underline{s}}_n) - d(\mathbf{\underline{s}}_{n'})\|) = \exp\{-\phi\|d(\mathbf{\underline{s}}_n) - d(\mathbf{\underline{s}}_{n'})\|\},$$

where $\phi > 0$ controls the spatial range.

Following Schmidt and O'Hagan (2003), the deformation process $d(\cdot)$ is modeled as a bivariate Gaussian process with prior

$$\mathbf{D} \sim \mathsf{Normal}_{2 \times N}(\mathbf{S}, \boldsymbol{\sigma}_d^2, \mathbf{R}_d),$$

where $\mathbf{S} = [\mathbf{s}_1 \cdots \mathbf{s}_N]$ is the $2 \times N$ matrix of observed coordinates, $\boldsymbol{\sigma}_d^2$ controls the scale of distortion in each spatial dimension, and \mathbf{R}_d encodes the prior correlation between sites in \mathcal{S} .

To avoid identifiability issues, σ_d^2 is taken as diagonal matrix (Schmidt and O'Hagan 2003). Since σ_d^2 is generally not well identified in practice, works such as Damian et al. (2001) and Morales and Vicini (2020) treat this matrix as fixed rather than estimated, thereby avoiding potential instability in posterior inference. In this paper, we work with the following specification:

$$\sigma_d^2 = \tau \cdot \operatorname{diag}\{\hat{\sigma}_{lon}^2, \hat{\sigma}_{lat}^2\}, \quad 0 < \tau \le 1,$$

where $\hat{\sigma}_{lon}^2$ and $\hat{\sigma}_{lat}^2$ are the sample variances of longitude and latitude, respectively. For \mathbf{R}_d , we adopt a Gaussian correlation function. Its general entry has the form

$$R_{n,n'} = \rho_{\psi}(\|\mathbf{\underline{s}}_n - \mathbf{\underline{s}}_{n'}\|) = \exp\{-\psi\|\mathbf{\underline{s}}_n - \mathbf{\underline{s}}_{n'}\|^2\},$$

with $\psi > 0$, so that geographically distant sites in \mathcal{S} have weaker prior correlation in \mathcal{D} . This prior formulation controls the smoothness of the deformation, allowing the latent space to stretch or compress according to the degree of anisotropy observed in the data.

2.3 Spatiotemporal hierarchical structure

The temporal evolution of the process is modeled through a Bayesian dynamic structure applied to the matrix-variate responses defined in Section 2.1. At each time t, the $N \times q$ response matrix \mathbf{Y}_t contains the q variables measured simultaneously across the N monitoring sites. Let $\mathbf{Y}_t = \text{vec}(\mathbf{Y}_t)$ denote its column-stacked vectorization.

Associated with each time t, we define a latent parameter matrix β_t of dimension $p \times q$, whose entries represent regression effects or latent states driving the temporal and

multivariate structure of the process. Its vectorized form $\beta_t = \text{vec}(\beta_t)$ evolves according to a first-order Markov model, where Σ captures contemporaneous dependence among variables and \mathbf{W} controls the temporal smoothness of the states.

The hierarchical model consists of three stages:

Observation equation. At each time t, the process \mathbf{Y}_t is related to the current state $\boldsymbol{\beta}_t$ through the design matrix \mathbf{X}_t (of dimension $N \times p$) and the spatial correlation structure \mathbf{B} specified by the spatial range ϕ and the deformations \mathbf{D} :

$$[\mathbf{Y}_t \mid \boldsymbol{\beta}_t, V, \phi, \mathbf{D}, \boldsymbol{\Sigma}] \sim \mathsf{Normal}_{Nq}([\mathbf{I}_q \otimes \mathbf{X}_t] \boldsymbol{\beta}_t, V \cdot [\boldsymbol{\Sigma} \otimes \mathbf{B}]),$$
 (2)

where V > 0 is a global scale parameter. This layer combines spatial, multivariate, and temporal components through the hierarchical dependency on β_t .

Evolution equation. The latent states evolve dynamically over time according to

$$[\boldsymbol{\beta}_t \mid \boldsymbol{\beta}_{t-1}, V, \boldsymbol{\Sigma}] \sim \mathsf{Normal}_{pq}([\mathbf{I}_q \otimes \mathbf{G}_t] \boldsymbol{\beta}_{t-1}, V \cdot [\boldsymbol{\Sigma} \otimes \mathbf{W}]),$$
 (3)

where \mathbf{G}_t $(p \times p)$ controls the temporal propagation of the states, and \mathbf{W} $(p \times p)$ governs their variability across time.

Initial information. The initial state β_0 follows

$$[\boldsymbol{\beta}_0 \mid V, \boldsymbol{\Sigma}] \sim \mathsf{Normal}_{pq}(\mathbf{M}_0, V \cdot [\boldsymbol{\Sigma} \otimes \mathbf{C}_0]),$$
 (4)

where \mathbf{M}_0 and \mathbf{C}_0 are prior mean and covariance matrices describing the initial uncertainty of the states.

The model integrates temporal, spatial, and multivariate components within a single hierarchical structure. Temporal dependence arises from the state-evolution equation (3), where the matrices \mathbf{G}_t and \mathbf{W} control, respectively, the persistence and variability of the dynamic coefficients over time. Spatial dependence is induced by the matrix \mathbf{B} , whose elements are defined in the deformed space \mathcal{D} described in Section 2.2, allowing for anisotropic spatial correlation among locations. The matrix $\mathbf{\Sigma}$ captures contemporaneous dependence among the q response variables, linking their joint variability at each time point.

Assuming prior independence among the components of $\{\phi, \mathbf{D}, V, \mathbf{\Sigma}\}\$ and applying the Markov property of the latent states, the joint prior distribution of the parameters can be written as

$$f(\boldsymbol{\theta}) = f(\phi)f(\mathbf{D})f(V)f(\boldsymbol{\Sigma})f(\boldsymbol{\beta}_0 \mid V, \boldsymbol{\Sigma}) \prod_{t=1}^{T} f(\boldsymbol{\beta}_t \mid \boldsymbol{\beta}_{t-1}, V, \boldsymbol{\Sigma}), \tag{5}$$

where $\boldsymbol{\theta} = \{ \underline{\beta}_{0:T}, V, \boldsymbol{\Sigma}, \phi, \mathbf{D} \}$ with $\underline{\beta}_{0:T} = \{ \underline{\beta}_1, \dots, \underline{\beta}_T \}$ denotes the complete set of model parameters.

Given conditional independence of the observations across time, the likelihood function is expressed as

$$l(\boldsymbol{\theta}; \mathbf{y}) = \prod_{t=1}^{T} f(\mathbf{y}_t \mid \boldsymbol{\beta}_t, V, \phi, \mathbf{D}, \boldsymbol{\Sigma}),$$
(6)

and combining (5) and (6) through Bayes' theorem yields the posterior density

$$f(\boldsymbol{\theta} \mid \mathbf{y}) \propto f(\phi) f(\mathbf{D}) f(V) f(\boldsymbol{\Sigma}) f(\boldsymbol{\beta}_0 \mid V, \boldsymbol{\Sigma}) \times \prod_{t=1}^{T} f(\boldsymbol{\beta}_t \mid \boldsymbol{\beta}_{t-1}, V, \boldsymbol{\Sigma}) f(\mathbf{y}_t \mid \boldsymbol{\beta}_t, V, \phi, \mathbf{D}, \boldsymbol{\Sigma}).$$
(7)

This formulation extends isotropic matrix-variate dynamic models by introducing anisotropic spatial structures through the deformation \mathbf{D} , while maintaining tractability for posterior inference via the Markov chain Monte Carlo (MCMC) algorithms described in Section 2.4.

2.4 Parameter estimation

The posterior distribution in (7) does not have a closed analytical form. Inference is therefore performed using an MCMC algorithm that combines Gibbs sampling for parameters with known full conditionals and Metropolis–Hastings, slice-sampling, or FFBS (Forward Filtering, Backward Sampling) updates for those without closed forms. This hybrid procedure generates draws from the joint posterior distribution of all model parameters, allowing full Bayesian inference.

2.4.1 Full conditional distributions

Scale parameter V. We assign an inverse-gamma prior

$$V \sim \text{Inverse-Gamma}(a_V, b_V),$$

where $a_V > 0$ and $b_V > 0$ denote the shape and scale parameters. Given the conjugacy of the model, the full conditional distribution of V is also inverse-gamma:

$$[V \mid \mathbf{\hat{y}} = \mathbf{y}, \boldsymbol{\beta}_{0:T}, \boldsymbol{\Sigma}, \phi, \mathbf{D}] \sim \mathsf{Inverse-Gamma}(a'_V, b'_V),$$

where the updated parameters a'_V and b'_V are given in Appendix A.1.

Contemporaneous covariance Σ . When the $q \times q$ covariance matrix Σ is unrestricted, we assign an inverse-Wishart prior

$$\Sigma \sim \text{Inverse-Wishart}_a(a_{\Sigma}, \mathbf{b}_{\Sigma}),$$

where $a_{\Sigma} > q - 1$ represents the degrees of freedom and $\mathbf{b}_{\Sigma} \in \operatorname{Sym}^+(q)$ is the scale matrix. Here, $\mathbf{A} \in \operatorname{Sym}^+(q)$ indicates that a $q \times q$ matrix \mathbf{A} is symmetric positive definite. The conjugate full conditional distribution is also inverse-Wishart:

$$[\Sigma \mid \mathbf{Y} = \mathbf{y}, \boldsymbol{\beta}_{0:T}, V, \phi, \mathbf{D}] \sim \mathsf{Inverse-Wishart}_q(a'_{\Sigma}, \mathbf{b}'_{\Sigma}),$$

with a'_{Σ} and \mathbf{b}'_{Σ} as given in Appendix A.2.1.

When independence among response variables is assumed, Σ is taken as diagonal,

$$\Sigma = \operatorname{diag}\{\Sigma_{1,1}, \dots, \Sigma_{q,q}\},\$$

and each diagonal element follows an independent inverse-gamma prior

$$\Sigma_{i,i} \sim \mathsf{Inverse-Gamma}(a_{\Sigma_{i,i}}, b_{\Sigma_{i,i}}),$$

the corresponding full conditional distributions are also inverse-gamma:

$$[\Sigma_{i,i} \mid \mathbf{Y} = \mathbf{y}, \boldsymbol{\beta}_{0:T}, V, \phi, \mathbf{D}] \sim \mathsf{Inverse-Gamma}(a'_{\Sigma_{i,i}}, b'_{\Sigma_{i,i}}), \quad i \in \{1, \dots, q\},$$

with $a'_{\Sigma_{i,i}}$ and $b'_{\Sigma_{i,i}}$ as given in Appendix A.2.2. This diagonal case serves as a benchmark model assuming conditional independence across response variables.

Dynamic coefficients β_t . The latent state vectors $\beta_{0:T} = \{\beta_0, \beta_1, \dots, \beta_T\}$ are jointly updated using the FFBS algorithm (Frühwirth-Schnatter 1994; Carter and Kohn 1994; Chib and Greenberg 1995), which performs exact simulation in Gaussian state-space models. The joint conditional distribution is proportional to

$$f(\underline{\beta}_{0:T} \mid \underline{\mathbf{y}}, \phi, \mathbf{D}, V, \underline{\boldsymbol{\Sigma}}) \propto f(\underline{\beta}_0 \mid V, \underline{\boldsymbol{\Sigma}}) \prod_{t=1}^T f(\underline{\beta}_t \mid \underline{\beta}_{t-1}, V, \underline{\boldsymbol{\Sigma}}) f(\underline{\mathbf{y}}_t \mid \underline{\beta}_t, V, \phi, \underline{\mathbf{D}}, \underline{\boldsymbol{\Sigma}}),$$
(8)

and the FFBS algorithm alternates Kalman filtering with backward sampling to generate full trajectories of β_t conditional on the data and parameters.

Spatial range parameter ϕ **.** The spatial range parameter ϕ controls the rate of decay of spatial correlation in the deformed space. Following Fonseca and Steel (2011, Sec. 4), we assign a gamma prior

$$\phi \sim \mathsf{Gamma}(1, 0.3/\zeta),$$

where $\mathsf{Gamma}(a,b)$ denotes the Gamma distribution with shape a>0 and rate b>0, and ζ is the median Euclidean distance between all pairs of gauged sites in \mathcal{S} . Because the full conditional distribution has no closed form, ϕ is updated through a Metropolis–Hastings step (Gamerman and Lopes 2006, Chap. 6), with log-target density

$$\ln f(\phi \mid \mathbf{y}, \boldsymbol{\beta}_{0:T}, V, \boldsymbol{\Sigma}, \mathbf{D}) = \text{Constant} - \frac{0.3\phi}{\zeta} - \frac{Tq}{2} \ln(\det \mathbf{B})$$
$$- \frac{1}{2V} \sum_{t=1}^{T} \left(\mathbf{y}_{t} - [\mathbf{I}_{q} \otimes \mathbf{X}_{t}] \boldsymbol{\beta}_{t} \right)^{\top} [\boldsymbol{\Sigma} \otimes \mathbf{B}]^{-1} \left(\mathbf{y}_{t} - [\mathbf{I}_{q} \otimes \mathbf{X}_{t}] \boldsymbol{\beta}_{t} \right). \quad (9)$$

Deformation process D. Following Schmidt and O'Hagan (2003), the latent deformation matrix **D** is assigned a matrix-normal prior

$$\mathbf{D} \sim \mathsf{Normal}_{2 \times N}(\mathbf{S}, \boldsymbol{\sigma}_d^2, \mathbf{R}_d),$$

where \mathbf{S} , $\boldsymbol{\sigma}_d^2$, and \mathbf{R}_d are described in Section 2.2. The full conditional distribution has no closed form, with log-density given by

$$\ln f(\mathbf{D} \mid \mathbf{y}, \boldsymbol{\beta}_{0:T}, V, \boldsymbol{\Sigma}, \phi) = \text{Constant} - \frac{1}{2} \operatorname{tr} \left[(\mathbf{D} - \mathbf{S})^{\top} \boldsymbol{\sigma}_{d}^{-2} (\mathbf{D} - \mathbf{S}) \mathbf{R}_{d}^{-1} \right]$$

$$- \frac{Tq}{2} \ln(\det \mathbf{B}) - \frac{1}{2V} \sum_{t=1}^{T} \left(\mathbf{y}_{t} - [\mathbf{I}_{q} \otimes \mathbf{X}_{t}] \boldsymbol{\beta}_{t} \right)^{\top} [\boldsymbol{\Sigma} \otimes \mathbf{B}]^{-1} \left(\mathbf{y}_{t} - [\mathbf{I}_{q} \otimes \mathbf{X}_{t}] \boldsymbol{\beta}_{t} \right). \quad (10)$$

Because **B** depends nonlinearly on the distances in the deformed space, **D** is updated component-wise using the univariate slice sampler (Neal 2003). In the isotropic case, deformation is suppressed by setting $d(\underline{s}) = \underline{s}$, providing a baseline for model comparison.

Regarding the spatial component, note that $B_{n,n'} = \exp\{-\phi \| d(\mathbf{g}_n) - d(\mathbf{g}_{n'}) \|\}$ is a strictly decreasing function of the distance in the deformed space. As a result, the covariance structure defined by \mathbf{B} is unique up to a scaling factor, and the deformation $d(\cdot)$ is unique up to homothetic transformations (Perrin and Meiring 1999). Following standard practice in Bayesian spatial deformation models (Damian et al. 2001; Morales et al. 2013; Gamerman et al. 2024; Sampson and Meiring 2014), the locations of two sites in \mathcal{D} are fixed to avoid the remaining indeterminacy and ensure identifiability.

Finally, the parameters V and Σ are not separately identifiable. For any constant $\kappa > 0$, the models

$$\mathsf{Normal}_{Nq} \big([\mathbf{I}_q \otimes \mathbf{X}_t] \boldsymbol{\beta}_t, V[\boldsymbol{\Sigma} \otimes \mathbf{B}] \big) \text{ and } \mathsf{Normal}_{Nq} \big([\mathbf{I}_q \otimes \mathbf{X}_t] \boldsymbol{\beta}_t, (V/\kappa)[\{\kappa \boldsymbol{\Sigma}\} \otimes \mathbf{B}] \big)$$

are equivalent. Hence, V and Σ cannot be independently identified, although their product $V\Sigma$ is identifiable and represents the overall scale of variability in the model.

2.4.2 Hybrid algorithm

A hybrid MCMC algorithm is employed to generate samples from the posterior distribution of the set of parameters $\boldsymbol{\theta} = \{\boldsymbol{\beta}_{0:T}, V, \boldsymbol{\Sigma}, \phi, \mathbf{D}\}$. The algorithm combines Gibbs sampling with FFBS, slice sampling, and Metropolis–Hastings updates to efficiently explore the joint posterior space.

After convergence is achieved (say after J iterations), the algorithm is used to store K posterior draws of the unknown quantities, denoted by $\boldsymbol{\theta}^{(j_1)}, \dots, \boldsymbol{\theta}^{(j_K)}$, where

the indices satisfy $J+1 \leq j_1 < \cdots < j_K$. Thinning may be applied to reduce autocorrelation in the retained samples.

The full procedure is summarized in Algorithms 1 and 2.

3 Model for incomplete matrix-variate responses

3.1 General framework

We allow each $N \times q$ response matrix \mathbf{Y}_t to contain missing entries. Let N_t^{obs} and N_t^{mis} denote, respectively, the numbers of observed and missing elements at time t, satisfying $N_t^{\mathsf{obs}} + N_t^{\mathsf{mis}} = Nq$. Depending on the pattern of availability, each matrix \mathbf{Y}_t can fall into one of three categories: (i) fully observed $(N_t^{\mathsf{obs}} = Nq)$, (ii) partially observed $(0 < N_t^{\mathsf{obs}} < Nq)$, and (iii) fully missing $(N_t^{\mathsf{obs}} = 0)$.

Let $\mathcal{T}_{complete}$, $\mathcal{T}_{partial}$, and $\mathcal{T}_{missing}$ denote the sets of time indices corresponding to the three situations above. The complete set of time indices is then the disjoint union $\mathcal{T} = \mathcal{T}_{complete} \cup \mathcal{T}_{partial} \cup \mathcal{T}_{missing}$. Following Gamerman et al. (2022), the missing-data mechanism is assumed to be completely at random.

When \mathbf{Y}_t is partially observed, the missing pattern may not correspond to contiguous blocks within the matrix. It is therefore convenient to work with the vectorized form $\mathbf{Y}_t = \text{vec}(\mathbf{Y}_t)$, which allows us to separate observed and missing components using a permutation. For illustration, consider N = 4 and q = 2:

$$\mathbf{Y}_{t} = \begin{bmatrix} Y_{1,1,t}^{\text{obs}} & Y_{1,2,t}^{\text{mis}} \\ Y_{2,1,t}^{\text{obs}} & Y_{2,2,t}^{\text{mis}} \\ Y_{3,1,t}^{\text{mis}} & Y_{3,2,t}^{\text{obs}} \\ Y_{4,1,t}^{\text{obs}} & Y_{4,2,t}^{\text{obs}} \end{bmatrix}^{\top}.$$

$$\mathbf{Y}_{t} = \begin{bmatrix} Y_{1,1,t}^{\text{obs}} & Y_{2,1,t}^{\text{obs}} & Y_{3,1,t}^{\text{obs}} & Y_{1,2,t}^{\text{mis}} & Y_{3,2,t}^{\text{obs}} & Y_{4,2,t}^{\text{obs}} \end{bmatrix}^{\top}.$$

Let \mathbf{P}_t be the $Nq \times Nq$ permutation matrix that rearranges \mathbf{Y}_t so that observed elements come first:

$$\mathbf{P}_t \mathbf{\tilde{Y}}_t = \begin{bmatrix} \mathbf{\tilde{Y}}_{t, \mathsf{obs}} \\ \mathbf{Y}_{t, \mathsf{mis}} \end{bmatrix}, \quad \mathbf{L}_{t, \mathsf{obs}} = \begin{bmatrix} \mathbf{I}_{N_t^{\mathsf{obs}}} & \mathbf{0} \end{bmatrix}, \quad \mathbf{L}_{t, \mathsf{mis}} = \begin{bmatrix} \mathbf{0} & \mathbf{I}_{N_t^{\mathsf{mis}}} \end{bmatrix},$$

so that $\mathbf{Y}_{t,\mathsf{obs}} = \mathbf{L}_{t,\mathsf{obs}} \mathbf{P}_t \mathbf{Y}_t$ and $\mathbf{Y}_{t,\mathsf{mis}} = \mathbf{L}_{t,\mathsf{mis}} \mathbf{P}_t \mathbf{Y}_t$. Intuitively, \mathbf{P}_t reorders the entries to place observed components first, and $\mathbf{L}_{t,\mathsf{obs}}$ and $\mathbf{L}_{t,\mathsf{mis}}$ then extract the observed and missing subvectors, respectively. If $t \in \mathcal{T}_{\mathsf{complete}}$, then $\mathbf{P}_t = \mathbf{I}_{Nq}$ and $\mathbf{Y}_{t,\mathsf{obs}} = \mathbf{Y}_t$.

From the observation model in (2), define

$$m{ ilde{\mu}}_t = \mathbf{P}_t[\mathbf{I}_q \otimes \mathbf{X}_t] \hat{m{eta}}_t = egin{bmatrix} m{\mu}_{t,\mathsf{obs}} \ \hat{m{\mu}}_{t,\mathsf{mis}} \end{bmatrix}, \qquad m{\Delta}_t = \mathbf{P}_t[m{\Sigma} \otimes \mathbf{B}] \mathbf{P}_t^ op = egin{bmatrix} m{\Delta}_{t,\mathsf{obs}} & m{\Delta}_{t,\mathsf{o,m}} \ m{\Delta}_{t,\mathsf{mis}} \end{bmatrix},$$

where $\underline{\mu}_{t,\text{obs}} = \mathbf{L}_{t,\text{obs}}\underline{\mu}_t$ and $\underline{\mu}_{t,\text{mis}} = \mathbf{L}_{t,\text{mis}}\underline{\mu}_t$, with analogous definitions for the covariance blocks. Then,

$$\left[\begin{bmatrix} \mathbf{Y}_{t, \text{obs}} \\ \mathbf{\tilde{Y}}_{t, \text{mis}} \end{bmatrix} \middle| \boldsymbol{\beta}_t, V, \boldsymbol{\phi}, \mathbf{D}, \boldsymbol{\Sigma} \right] \sim \text{Normal}_{N_t^{\text{obs}} + N_t^{\text{mis}}} \left(\begin{bmatrix} \boldsymbol{\mu}_{t, \text{obs}} \\ \boldsymbol{\tilde{\mu}}_{t, \text{mis}} \end{bmatrix}, V \cdot \begin{bmatrix} \boldsymbol{\Delta}_{t, \text{obs}} & \boldsymbol{\Delta}_{t, \text{o,m}} \\ \boldsymbol{\Delta}_{t, \text{m,o}} & \boldsymbol{\Delta}_{t, \text{mis}} \end{bmatrix} \right).$$
 (11)

The conditional distribution of the missing vector follows from the standard partition result of the multivariate Normal distribution (West and Harrison 1997, Sec. 17.2.2). Specifically,

$$[\mathbf{\underline{Y}}_{t,\text{mis}} \mid \mathbf{\underline{Y}}_{t,\text{obs}} = \mathbf{\underline{y}}_{t,\text{obs}}, \boldsymbol{\theta}] \sim \text{Normal}_{N_t^{\text{mis}}} (\mathbf{\underline{\mu}}_{\mathbf{\underline{Y}}_{t,\text{mis}}|\mathbf{\underline{Y}}_{t,\text{obs}}}, V \cdot \boldsymbol{\Delta}_{\mathbf{\underline{Y}}_{t,\text{mis}}|\mathbf{\underline{Y}}_{t,\text{obs}}}), \tag{12}$$

where

$$\underline{\boldsymbol{\mu}}_{\mathbf{Y}_{t,\mathrm{mis}}|\mathbf{Y}_{t,\mathrm{obs}}} = \underline{\boldsymbol{\mu}}_{t,\mathrm{mis}} + \boldsymbol{\Delta}_{t,\mathrm{m,o}} \boldsymbol{\Delta}_{t,\mathrm{obs}}^{-1} \big(\underline{\mathbf{y}}_{t,\mathrm{obs}} - \underline{\boldsymbol{\mu}}_{t,\mathrm{obs}} \big),$$
 (13)

$$\Delta_{\mathbf{Y}_{t,\mathsf{mis}}|\mathbf{Y}_{t,\mathsf{obs}}} = \Delta_{t,\mathsf{mis}} - \Delta_{t,\mathsf{m},\mathsf{o}} \Delta_{t,\mathsf{obs}}^{-1} \Delta_{t,\mathsf{o},\mathsf{m}}. \tag{14}$$

Marginally,

$$[\mathbf{\hat{Y}}_{t,\mathsf{mis}} \mid \boldsymbol{\theta}] \sim \mathsf{Normal}_{N_{\star}^{\mathsf{mis}}}(\boldsymbol{\mu}_{t,\mathsf{mis}}, V \cdot \boldsymbol{\Delta}_{t,\mathsf{mis}}).$$
 (15)

Collect all partially or fully missing vectors as

$$\mathbf{Y}_{\mathsf{mis}} = \{\mathbf{Y}_{t,\mathsf{mis}} : 0 < N_t^{\mathsf{mis}} \leq Nq\}, \qquad \mathbf{Y}_{\mathsf{obs}} = \{\mathbf{Y}_{t,\mathsf{obs}} : N_t^{\mathsf{obs}} > 0\}.$$

Assuming conditional independence across time,

$$f(\mathbf{\underline{y}}_{\mathsf{mis}} \mid \boldsymbol{\theta}, \mathbf{\underline{y}}_{\mathsf{obs}}) = \prod_{t \in \mathcal{T}_{\mathsf{partial}}} f(\mathbf{\underline{y}}_{t,\mathsf{mis}} \mid \mathbf{\underline{y}}_{t,\mathsf{obs}}, \boldsymbol{\theta}) \prod_{t \in \mathcal{T}_{\mathsf{missing}}} f(\mathbf{\underline{y}}_{t,\mathsf{mis}} \mid \boldsymbol{\theta}), \tag{16}$$

with support

$$\mathcal{Y}_{\mathsf{mis}} = \left(\prod_{t \in \mathcal{T}_{\mathrm{partial}}} \mathbb{R}^{N_t^{\mathsf{mis}}} \right) imes \left(\prod_{t \in \mathcal{T}_{\mathrm{missing}}} \mathbb{R}^{Nq}
ight).$$

Algorithm 3 samples from (16) using Monte Carlo simulation. Intuitively, this step imputes the missing values by drawing from their conditional Gaussian distributions, which automatically incorporate spatial, temporal, and cross-variable correlations through Δ_t .

3.2 Data augmentation method

The data augmentation approach offers an efficient strategy for posterior inference in models with incomplete data, where the likelihood factorizes in terms of observed and missing components (\mathbf{y}_{obs} and \mathbf{y}_{mis} , respectively). Posterior samples of the parameters and unobserved values are obtained by alternately drawing $\boldsymbol{\theta}$ and \mathbf{y}_{mis} , as described in Algorithms 4 and 5. After convergence—typically after J iterations—we retain K

posterior draws $\{\boldsymbol{\theta}^{(j_k)}, \mathbf{y}_{\mathsf{mis}}^{(j_k)}\}_{k=1}^K$, with $J+1 \leq j_1 < \cdots < j_K$; thinning may be applied to reduce autocorrelation within the chains.

Conceptually, this scheme treats the missing responses as latent variables, allowing joint estimation and imputation within a coherent Bayesian framework.

4 Interpolation

This section addresses the prediction of responses at N^* ungauged sites $\underline{s}_{N+1}, \ldots, \underline{s}_{N+N^*}$ within the spatial domain S. Let \mathbf{S}^* denote the $2 \times N^*$ matrix collecting these new locations, and let \mathbf{D}^* represent their corresponding coordinates in the deformed space \mathcal{D} , where $\underline{\mathbf{d}}_{N+n} = d(\underline{s}_{N+n})$ for $n \in \{1, \ldots, N^*\}$. Conditional on \mathbf{D} , the matrix-normal prior for \mathbf{D}^* implies

$$\left[\mathbf{D}^* \mid \mathbf{D}\right] \sim \mathsf{Normal}_{2 \times N^*} \left(\mathbf{S}^* + (\mathbf{D} - \mathbf{S}) \mathbf{R}_d^{-1} \mathbf{R}_{\mathsf{g},\mathsf{u}}, \boldsymbol{\sigma}_d^2, \mathbf{R}_d^* - \mathbf{R}_{\mathsf{u},\mathsf{g}} \mathbf{R}_d^{-1} \mathbf{R}_{\mathsf{g},\mathsf{u}}\right), \tag{17}$$

where \mathbf{R}_d , \mathbf{R}_d^* , and $\mathbf{R}_{\mathsf{g},\mathsf{u}}$ are correlation matrices constructed using a Gaussian kernel with range parameter ψ . Equation (17) propagates the estimated spatial deformation to the ungauged sites, effectively weighting the mapping according to proximity in the geographic domain \mathcal{S} .

Given \mathbf{D}^* , the joint Gaussian model for $(\mathbf{Y}_t, \mathbf{Y}_t^*)$ leads to the usual conditional formulation:

$$\left[\mathbf{\underline{Y}}_{t}^{*} \mid \mathbf{\underline{Y}}_{t}, \boldsymbol{\theta}, \mathbf{D}^{*}\right] \sim \mathsf{Normal}_{N^{*}q}\left(\mu_{\mathbf{Y}_{t}^{*}|\mathbf{Y}_{t}}, V \cdot \Delta_{\mathbf{\underline{Y}}_{t}^{*}|\mathbf{\underline{Y}}_{t}}\right),\tag{18}$$

with

$$\begin{split} & \underline{\boldsymbol{\mu}}_{\mathbf{Y}_t^*|\mathbf{Y}_t} = [\mathbf{I}_q \otimes \mathbf{X}_t^*] \underline{\boldsymbol{\beta}}_t + \mathbf{B}_{\mathsf{u},\mathsf{g}} \mathbf{B}^{-1} \big(\mathbf{Y}_t - [\mathbf{I}_q \otimes \mathbf{X}_t] \underline{\boldsymbol{\beta}}_t \big), \\ & \underline{\boldsymbol{\Delta}}_{\mathbf{Y}_t^*|\mathbf{Y}_t} = \underline{\boldsymbol{\Sigma}} \otimes (\mathbf{B}^* - \mathbf{B}_{\mathsf{u},\mathsf{g}} \mathbf{B}^{-1} \mathbf{B}_{\mathsf{g},\mathsf{u}}), \end{split}$$

where \mathbf{B} , \mathbf{B}^* , $\mathbf{B}_{\mathsf{u},\mathsf{g}}$, and $\mathbf{B}_{\mathsf{g},\mathsf{u}}$ are spatial correlation matrices derived from deformed distances using the kernel with range parameter ϕ . In practice, prediction at each ungauged location combines two components: a regression term $[\mathbf{I}_q \otimes \mathbf{X}_t^*] \hat{\boldsymbol{\beta}}_t$ representing the large-scale trend, and a kriging-type correction $\mathbf{B}_{\mathsf{u},\mathsf{g}} \mathbf{B}^{-1}(\cdot)$ that borrows spatial information from the observed sites through the deformed space.

To embed the interpolation step within the hierarchical framework, the parameter set is augmented to $\boldsymbol{\theta}_{int} = \{\boldsymbol{\theta}, \boldsymbol{Y}_{mis}, \mathbf{D}^*\}$, and we define $\boldsymbol{Y}_{int} = \{\boldsymbol{Y}_t^*\}_{t=1}^T$. The corresponding predictive density can then be written as

$$f(\mathbf{\hat{y}}_{\mathsf{int}} \mid \mathbf{\hat{y}}_{\mathsf{obs}}) = \int_{\mathbf{\Theta}_{\mathsf{int}}} \left[\prod_{t=1}^{T} f(\mathbf{\hat{y}}_{t}^{*} \mid \mathbf{\hat{y}}_{t}, \boldsymbol{\theta}, \mathbf{D}^{*}) \right] f(\mathbf{D}^{*} \mid \mathbf{D}) f(\boldsymbol{\theta}, \mathbf{\hat{y}}_{\mathsf{mis}} \mid \mathbf{\hat{y}}_{\mathsf{obs}}) \boldsymbol{\partial} \boldsymbol{\theta}_{\mathsf{int}}.$$
(19)

Since the integral in (19) has no closed form, it is approximated via Monte Carlo simulation by extending the steps of Algorithm 5 (see Algorithm 6). At each iteration, $\{\mathbf{y}_{\mathsf{mis}}, \boldsymbol{\theta}\}$ are sampled, the deformation is propagated to \mathbf{D}^* using (17), and conditional samples of \mathbf{Y}_t^* are drawn using (18). By accumulating these samples across iterations, the algorithm yields posterior predictive distributions for the responses at ungauged sites.

5 Model comparison

To assess and compare the performance of alternative Bayesian spatiotemporal models, we consider both goodness-of-fit and predictive accuracy criteria. The first measures how well a model explains the observed data, while the second evaluates its ability to reproduce unobserved or interpolated responses.

The *Deviance Information Criterion* (DIC) is widely used for Bayesian model comparison (Spiegelhalter et al. 2002). It balances model fit and complexity, penalizing overparameterization, and is computed from posterior samples of the model deviance. Among competing models fitted to the same dataset, the one with the smallest DIC is expected to yield the best predictive performance for a replicate dataset with the same structure as the observed one (Tsiko 2015, Page 5).

Beyond overall fit, we also evaluate predictive performance at ungauged locations. Let $\hat{Y}_{N+n,i,t}^{[\alpha]}$ denote the α -percentile and $\bar{Y}_{N+n,i,t}$ the posterior mean of the interpolated samples $Y_{N+n,i,t}^{(j_1)},\ldots,Y_{N+n,i,t}^{(j_K)}$. Following Gelman et al. (2013, Sec. 18.1), define the inclusion indicator

$$O_{n,i,t} = \left\{ \begin{aligned} &1, \text{ if } Y_{n,i,t} \text{ is observed } (Y_{n,i,t} = Y_{n,i,t}^{\mathsf{obs}}), \\ &0, \text{ if } Y_{n,i,t} \text{ is missing } (Y_{n,i,t} = Y_{n,i,t}^{\mathsf{mis}} = \mathtt{NA}). \end{aligned} \right.$$

To quantify the sharpness and coverage of predictive intervals, we employ the *Interval Score* (IS) proposed by Winkler (1972). Lower values of IS indicate more accurate and better-calibrated predictive intervals (Rostami-Tabar and Rendon-Sanchez 2021, Sec. 3.4.2). The IS combines interval width and a penalty when the true value lies outside the predictive range. For each time t, it is given by

$$\mathrm{IS}_{N+n,i,t}^{[\alpha]} = \hat{Y}_{N+n,i,t}^{[1-\alpha/2]} - \hat{Y}_{N+n,i,t}^{[\alpha/2]} + \begin{cases} \frac{2}{\alpha} (\hat{Y}_{N+n,i,t}^{[\alpha/2]} - Y_{N+n,i,t}), & \text{if } Y_{N+n,i,t} < \hat{Y}_{N+n,i,t}^{[\alpha/2]}, \\ \frac{2}{\alpha} (Y_{N+n,i,t} - \hat{Y}_{N+n,i,t}^{[1-\alpha/2]}), & \text{if } Y_{N+n,i,t} > \hat{Y}_{N+n,i,t}^{[1-\alpha/2]}, \\ 0, & \text{otherwise}, \end{cases}$$

and its average across time is

$$\mathrm{IS}_{N+n,i}^{[\alpha]} = \frac{\sum\limits_{t=1}^{T} O_{N+n,i,t} \cdot \mathrm{IS}_{N+n,i,t}^{[\alpha]}}{\sum\limits_{t=1}^{T} O_{N+n,i,t}}.$$

We further evaluate predictive accuracy using the *Predictive Mean Squared Error* (PMSE), which measures the average squared difference between predicted and observed values across all N^* ungauged locations (Shen and Gelfand 2019; Morales et al. 2022). Models with smaller PMSE are preferred, as they produce more accurate

interpolations and predictions (Shen and Gelfand 2019, Sec. 4). It is defined as

$$PMSE = \frac{\sum_{n=1}^{N^*} \sum_{i=1}^{q} \sum_{t=1}^{T} O_{N+n,i,t} (\bar{Y}_{N+n,i,t} - Y_{N+n,i,t})^2}{\sum_{n=1}^{N^*} \sum_{i=1}^{q} \sum_{t=1}^{T} O_{N+n,i,t}}.$$

6 Simulation study

We conduct a simulation study to evaluate the practical benefits of the proposed model relative to simpler alternatives. In particular, we examine whether incorporating spatial deformation and cross-variable correlation improves parameter estimation and predictive performance. To this end, we generate synthetic anisotropic spatiotemporal data under controlled settings, varying the time series length and the fraction of missing observations. The results are then compared across four model specifications that differ in their treatment of anisotropy and multivariate dependence.

Competing models. The four models under comparison are defined as follows:

- \mathcal{M}_1 (no deformation, independent responses): $d(\mathbf{g}) = \mathbf{g}, \ \Sigma = \text{diag}\{\Sigma_{1,1}, \dots, \Sigma_{q,q}\}.$
- \mathcal{M}_2 (no deformation, correlated responses): $d(\mathbf{s}) = \mathbf{s}, \ \Sigma \neq \mathrm{diag}\{\Sigma_{1,1}, \dots, \Sigma_{q,q}\}$.
- \mathcal{M}_3 (deformation, independent responses): $d(\mathbf{s}) \neq \mathbf{s}, \ \Sigma = \text{diag}\{\Sigma_{1,1}, \dots, \Sigma_{q,q}\}.$
- \mathcal{M}_4 (deformation, correlated responses proposed model): $d(\underline{\mathbf{s}}) \neq \underline{\mathbf{s}}, \ \mathbf{\Sigma} \neq \mathrm{diag}\{\Sigma_{1,1}, \dots, \Sigma_{q,q}\}.$

Anisotropic data-generating mechanism. To simulate geometric anisotropy, we follow Maity and Sherman (2012, Sec. 4) and specify the exponential spatial kernel

$$\exp\left\{-\phi\sqrt{(\mathbf{\underline{s}}_n - \mathbf{\underline{s}}_{n'})^{\top}\mathbf{A}(\mathbf{\underline{s}}_n - \mathbf{\underline{s}}_{n'})}\right\},\tag{20}$$

where $\mathbf{A} \in \operatorname{Sym}^+(2)$ is a matrix that controls the orientation and magnitude of anisotropy. By writing $\mathbf{A} = \mathbf{\Lambda}^\top \mathbf{\Lambda}$, the structure in (20) is equivalent to an isotropic kernel in the linearly transformed coordinates $\mathbf{d} = \mathbf{\Lambda}\mathbf{s}$:

$$\exp\left\{-\phi\sqrt{(\mathbf{s}_n - \mathbf{s}_{n'})^{\top}\mathbf{A}(\mathbf{s}_n - \mathbf{s}_{n'})}\right\} = \exp\{-\phi\|\mathbf{\Lambda}\mathbf{s}_n - \mathbf{\Lambda}\mathbf{s}_{n'}\|\}$$
$$= \exp\{-\phi\|d(\mathbf{s}_n) - d(\mathbf{s}_{n'})\|\}.$$

Hence, $d(\mathbf{g}) = \mathbf{\Lambda}\mathbf{g}$ defines a deterministic deformation that induces anisotropy. Following Maity and Sherman (2012, Sec. 4), we adopt

$$\mathbf{A} = 9\mathbf{I}_2 - 4\mathbf{1}_{2\times 2}, \qquad \mathbf{\Lambda} = \begin{bmatrix} 1 & 0 \\ 0 & 3 \end{bmatrix} \begin{bmatrix} \cos(\pi/4) & \sin(\pi/4) \\ -\sin(\pi/4) & \cos(\pi/4) \end{bmatrix},$$

which stretches one spatial axis and rotates the field by 45°.

Design and evaluation targets. We consider q=2 response variables, time lengths $T\in\{100,500\}$, and p=2 regression coefficients per response and time. The process Y is simulated at N=16 equally spaced sites within the unit square, and jointly at $N^*=3$ additional unequally spaced sites for interpolation assessment. We compare models \mathcal{M}_1 – \mathcal{M}_4 in terms of (i) accuracy of parameter recovery and (ii) predictive performance at ungauged locations. Figure 1 illustrates the spatial domain, highlighting the two fixed anchor sites (\mathbf{s}_1 and \mathbf{s}_2), the remaining gauged locations ($\mathbf{s}_3,\ldots,\mathbf{s}_{16}$), and the ungauged sites $\mathbf{S}^*=[\mathbf{s}_{17}\ \mathbf{s}_{18}\ \mathbf{s}_{19}]$ used for evaluating interpolation.

Simulation protocol. Data generation and MCMC configuration details, including the construction of the deformation matrices, parameter settings, covariate generation, and missing-value imposition, are fully described in Appendix C. In brief, we simulate latent states and observations according to the model equations using the parameter values reported above, with varying time lengths $(T \in \{100, 500\})$ and missing-value fractions $(\gamma \in \{0.15, 0.30\})$. Each scenario produces complete and partially observed datasets, which are analyzed under models \mathcal{M}_1 – \mathcal{M}_4 using the same prior and MCMC specifications.

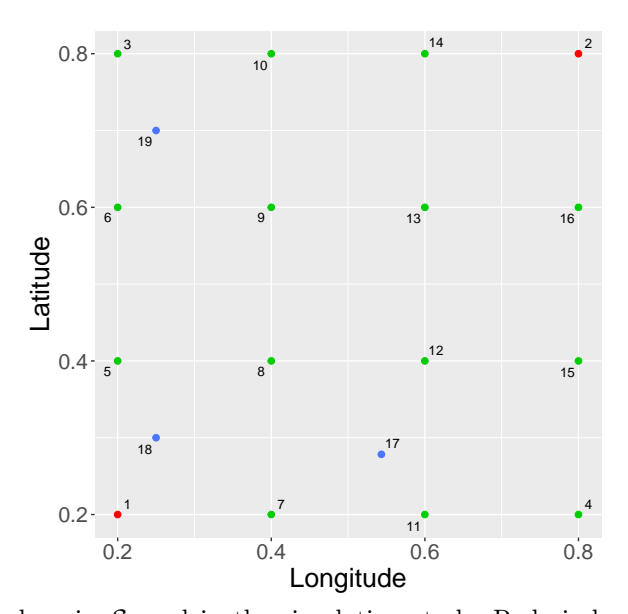


Fig. 1: Spatial domain S used in the simulation study. Red circles denote the two anchor sites $(\mathbf{g}_1 \text{ and } \mathbf{g}_2)$, green points represent the remaining gauged sites $(\mathbf{g}_3, \dots, \mathbf{g}_{16})$, and blue points correspond to the ungauged locations used for interpolation $(\mathbf{g}_{17}, \mathbf{g}_{18}, \mathbf{g}_{19})$.

To run Algorithm 5, we use the known matrices $\mathbf{G}_{1:T}$ and $\mathbf{X}_{1:T}$, and the observed subvectors $\mathbf{y}_{1,obs}, \dots, \mathbf{y}_{T,obs}$. We set the priors and state-evolution hyperparameters

as $a_V = 0.001$, $b_V = 0.001$, $a_{\Sigma} = 0.001$, $\mathbf{b}_{\Sigma} = 0.001\mathbf{I}_2$, $\mathbf{M}_0 = \mathbf{0}_{2\times 2}$, $\mathbf{C}_0 = \mathbf{I}_2$, $\mathbf{W} = \frac{0.05}{T}\mathbf{C}_0$, $\boldsymbol{\sigma}_d^2 = \mathrm{diag}\{\hat{\sigma}_{\mathrm{lon}}^2, \hat{\sigma}_{\mathrm{lat}}^2\}$, and $\psi = 10$.

We run Algorithm 5 for 20,000 iterations for \mathcal{M}_4 ; visual and numerical diagnostics indicate convergence after a burn-in of approximately $J \approx 5000$ iterations. The same configuration is used for the comparison models \mathcal{M}_1 – \mathcal{M}_3 . To reduce autocorrelation, we retain every 15th draw after burn-in, yielding K = 1000 posterior samples $\{\boldsymbol{\theta}^{(j_k)}, \mathbf{y}_{\mathsf{mis}}^{(j_k)}\}_{k=1}^K$ with indices $j_1 = 5001, j_2 = 5016, \ldots, j_{1000} = 19986$.

Tables 1–4 summarize, for each model and for all (T, γ) scenarios, the posterior mean, the 95% highest posterior density (HPD) interval, and the Geweke statistic for ϕ , $V\Sigma_{1,1}$, $V\Sigma_{1,2}$, and $V\Sigma_{2,2}$. We report $V\Sigma_{i,i'}$ rather than $(V, \Sigma_{i,i'})$ separately because V and Σ are not individually identifiable, whereas their product is.

Across all models, HPD intervals shrink with larger T and smaller missingness γ , as expected. Geweke statistics lie within (-1.96, 1.96) in all cases, indicating no evidence against convergence. The isotropic models \mathcal{M}_1 and \mathcal{M}_2 misestimate ϕ —their HPD intervals exclude the true value—while the anisotropic models \mathcal{M}_3 and \mathcal{M}_4 recover ϕ well when T=500. The variance-covariance products $V\Sigma_{1,1}$, $V\Sigma_{1,2}$, and $V\Sigma_{2,2}$ are accurately recovered by all models in every scenario. Estimates of the state coefficients $\beta_{0:T}$ are also accurate and similar across models; Figure 2 illustrates this for the trajectory of $\beta_{1,1,t}$ when T=100 and $\gamma=0.30$, showing posterior means closely tracking the truth with narrow 95% HPD bands.

Table 1: Posterior mean, 95% highest posterior density (HPD) interval, and Geweke statistic (GS) for the spatial range parameter ϕ , by model (\mathcal{M}_1 – \mathcal{M}_4), sample size ($T \in \{100, 500\}$), and missing-value fraction ($\gamma \in \{0.15, 0.30\}$). The true value is $\phi = 0.4$.

T	γ	Metric	\mathcal{M}_1	\mathcal{M}_2	\mathcal{M}_3	\mathcal{M}_4
100	0.15	Mean HPD GS	1.320 0.9363–1.6819 1.441	$\begin{array}{c} 1.216 \\ 0.8498 - 1.5312 \\ 1.251 \end{array}$	0.634 $0.4389-0.8403$ 0.795	0.585 $0.3987-0.7737$ 1.301
	0.30	Mean HPD GS	$\begin{array}{c} 1.292 \\ 0.9199 - 1.6672 \\ 0.847 \end{array}$	$\begin{array}{c} 1.207 \\ 0.8616 - 1.5564 \\ 1.187 \end{array}$	$0.622 \\ 0.4121 - 0.8370 \\ 1.224$	$0.571 \\ 0.3716 - 0.7532 \\ 1.432$
500	0.15	Mean HPD GS	$\begin{array}{c} 1.137 \\ 0.8460 - 1.4477 \\ 1.357 \end{array}$	$1.158 \\ 0.8544 - 1.4487 \\ 1.433$	$0.487 \\ 0.3421 - 0.6505 \\ 1.206$	0.495 $0.3435-0.6512$ 0.935
500	0.30	Mean HPD GS	$\begin{array}{c} 1.138 \\ 0.8361 - 1.4339 \\ 0.987 \end{array}$	$\begin{array}{c} 1.145 \\ 0.8481 - 1.4621 \\ 1.118 \end{array}$	0.495 $0.3382-0.6526$ 0.866	0.496 0.3355–0.6525 0.875

To evaluate how accurately the spatial deformation is recovered, we compute, for each anisotropic model \mathcal{M}_h $(h \in \{3,4\})$, the squared Frobenius norm between the

Table 2: Posterior mean, 95% HPD interval, and Geweke statistic (GS) for the parameter product $V\Sigma_{1,1}$, by model $(\mathcal{M}_1 - \mathcal{M}_4)$, sample size $(T \in \{100, 500\})$, and missing-value fraction $(\gamma \in \{0.15, 0.30\})$. The true value is $V\Sigma_{1,1} = 0.6$.

T	γ	Metric	\mathcal{M}_1	\mathcal{M}_2	\mathcal{M}_3	\mathcal{M}_4
100	0.15	Mean HPD GS	0.520 $0.3782-0.6879$ -1.045	0.550 $0.3956-0.7446$ -1.032	0.493 0.3485–0.6497 -0.609	0.524 0.3803-0.7093 -1.375
-00	0.30	Mean HPD GS	0.527 $0.3701-0.7058$ -0.497	0.546 0.3910-0.7347 -0.870	0.500 0.3488-0.6693 -0.799	0.522 0.3690-0.7070 -1.237
500	0.15	Mean HPD GS	0.546 $0.4069-0.7257$ -1.204	0.533 $0.4069-0.7333$ -1.178	0.531 $0.3928-0.7027$ -1.280	0.517 0.3857–0.6817 -1.012
500	0.30	Mean HPD GS	0.544 $0.4008-0.7258$ -0.721	0.537 $0.4042-0.7287$ -0.824	0.529 0.3889–0.7049 -0.573	0.516 0.3817–0.6818 -0.811

Table 3: Posterior mean, 95% HPD interval, and Geweke statistic (GS) for the parameter product $V\Sigma_{1,2}$, under models \mathcal{M}_2 and \mathcal{M}_4 , for different sample sizes ($T \in \{100, 500\}$) and missing-value fractions ($\gamma \in \{0.15, 0.30\}$). The true value is $V\Sigma_{1,2} = 0.51$.

T	γ	Metric	\mathcal{M}_2	\mathcal{M}_4
100	0.15	Mean HPD GS	0.463 $0.3233-0.6259$ -1.254	0.443 $0.3134-0.6108$ -1.599
100	0.30	Mean HPD GS	0.457 $0.3213-0.6353$ -1.047	0.436 0.3146–0.6134 -1.435
500	0.15	Mean HPD GS	0.444 0.3344-0.6114 -1.367	0.432 0.3192-0.5851 -1.233
500	0.30	Mean HPD GS	0.451 $0.3320-0.6116$ -1.030	0.432 0.3232-0.5922 -1.057

true deformation matrix **D** and its estimate at the kth MCMC iteration, $\mathbf{D}_{\mathcal{M}_k}^{(j_k)}$:

$$\|\mathbf{D} - \mathbf{D}_{\mathcal{M}_h}^{(j_k)}\|_{\mathrm{F}}^2 = \mathrm{tr} \Big[(\mathbf{D} - \mathbf{D}_{\mathcal{M}_h}^{(j_k)}) (\mathbf{D} - \mathbf{D}_{\mathcal{M}_h}^{(j_k)})^{\top} \Big] \,.$$

Table 4: Posterior mean, 95% HPD interval, and Geweke statistic (GS) for the parameter product $V\Sigma_{2,2}$, by model $(\mathcal{M}_1 - \mathcal{M}_4)$, sample size $(T \in \{100, 500\})$, and missing-value fraction $(\gamma \in \{0.15, 0.30\})$. The true value is $V\Sigma_{2,2} = 0.6$.

T	γ	Metric	\mathcal{M}_1	\mathcal{M}_2	\mathcal{M}_3	\mathcal{M}_4
100	0.15	Mean HPD GS	0.512 $0.3643-0.6920$ -1.163	0.545 $0.3912-0.7488$ -1.427	0.488 $0.3440-0.6557$ -0.796	0.523 0.3779–0.7250 -1.789
	0.30	Mean HPD GS	0.508 0.3630–0.7035 -1.214	0.538 0.3865–0.7510 -1.434	0.481 0.3395–0.6532 -1.915	0.514 0.3560–0.6995 -1.855
500	0.15	Mean HPD GS	0.532 $0.3970-0.7039$ -1.520	0.522 $0.3825-0.6923$ -1.547	0.527 $0.3900-0.6838$ -1.522	0.511 0.3855–0.6838 -1.109
500	0.30	Mean HPD GS	0.539 $0.4017-0.7340$ -1.684	$0.533 \\ 0.3919 - 0.7141 \\ -1.128$	0.533 $0.3971-0.7079$ -1.362	0.517 0.3751–0.6945 -1.473

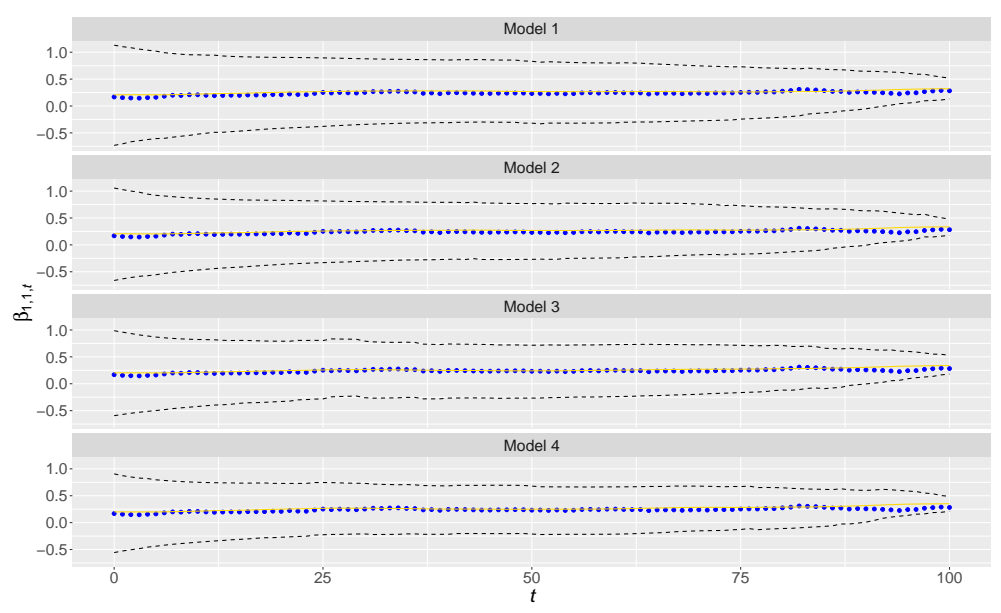


Fig. 2: Posterior distribution of $\beta_{1,1,t}$ for $t \in \{1,\ldots,100\}$ by model, from the simulation study with T=100 and $\gamma=0.30$. Black dashed lines denote 95% HPD intervals, the solid golden line represents the posterior mean, and points indicate the true values.

Table 5 reports posterior summaries (mean, 95% HPD interval, and Geweke statistic) of this squared distance, by anisotropic model (\mathcal{M}_3 and \mathcal{M}_4), sample size ($T \in \{100, 500\}$), and missing-value fraction ($\gamma \in \{0.15, 0.30\}$). As expected, the

estimated deformations approach the true one as the sample size increases and the proportion of missing data decreases. Figure 3a shows the true deformation used to generate the data; Figure 3b displays the estimate obtained under Model 3 for T=100 and $\gamma=0.30$, representing a low-information case; and Figure 3c shows the estimate from Model 4 for T=500 and $\gamma=0.15$, the most favorable scenario. Both the numerical results and visual inspection confirm that the deformation is poorly recovered for small T but closely approximated under larger samples.

Table 5: Posterior mean, 95% HPD interval, and Geweke statistic (GS) of the squared Frobenius norm between the true and estimated deformation, by model (\mathcal{M}_3 and \mathcal{M}_4), sample size ($T \in \{100, 500\}$), and missing-value fraction ($\gamma \in \{0.15, 0.30\}$).

T	γ	Metric	\mathcal{M}_3	\mathcal{M}_4
100	0.15	Mean HPD GS	1.019 0.3061–2.0078 -0.887	0.960 $0.1350-2.3898$ 0.361
200	0.30	Mean HPD GS	1.074 0.2882–2.3670 -0.309	0.953 0.2085–1.9147 -0.268
500	0.15	Mean HPD GS	0.222 0.0400-0.4936 0.177	0.230 0.0296–0.5711 -1.283
	0.30	Mean HPD GS	0.274 $0.0485 - 0.6584$ 1.045	0.307 0.0540–0.7259 0.008

Table 6 summarizes the model comparison metrics. According to the DIC statistic, the proposed model \mathcal{M}_4 provides the best overall fit across all sample sizes and levels of missingness. It also yields the smallest PMSE values in every scenario, confirming its superior predictive accuracy for interpolation. The results suggest that accounting for cross-variable dependence ($\Sigma \neq \text{diag}\{\Sigma_{1,1},\ldots,\Sigma_{q,q}\}$) contributes primarily to the improvement in model fit, as reflected by lower DIC values, whereas incorporating spatial deformation ($d(\underline{\mathbf{s}}) \neq \underline{\mathbf{s}}$) plays a key role in reducing the PMSE, thereby enhancing predictive performance.

Table 7 reports the interval score (IS) values by ungauged site, response variable, sample size, and missing-value fraction. Consistently, the proposed model \mathcal{M}_4 achieves the lowest IS values, indicating the most accurate and well-calibrated predictive intervals, while the simplest specification \mathcal{M}_1 performs worst, as expected. These findings are visually reinforced in Figure 4, which compares the interpolations at the ungauged location \mathbf{g}_{17} for the first response variable. Model \mathcal{M}_4 not only provides predictions closest to the true values but also exhibits slightly narrower 95% credibility intervals, in full agreement with the numerical results from the IS and PMSE analyses.

Table 6: Metrics for model comparison (DIC and PMSE) for different sample sizes $(T \in \{100, 500\})$ and fractions of missing values $(\gamma \in \{0.15, 0.30\})$, resulting from the simulation study.

T	γ	Metric	\mathcal{M}_1	\mathcal{M}_2	\mathcal{M}_3	\mathcal{M}_4
100	0.15	DIC PMSE	$3379.1 \\ 0.0584$	$1530.5 \\ 0.0573$	$2616.4 \\ 0.0505$	$725.6 \\ 0.0501$
	0.30	DIC PMSE	2858.9 0.0652	1201.7 0.0610	2212.9 0.0566	524.9 0.0526
500	0.15	DIC PMSE	15900.6 0.0590	6815.4 0.0558	11989.3 0.0512	2852.7 0.0488
500	0.30	DIC PMSE	13675.1 0.0649	5561.0 0.0585	$10436.4 \\ 0.0558$	2366.8 0.0509

In summary, the simulation study demonstrates that, for data exhibiting geometric anisotropy of the type considered here, the proposed model (\mathcal{M}_4) yields more accurate parameter estimates and superior interpolation performance than the competing alternatives $(\mathcal{M}_1 - \mathcal{M}_3)$.

7 Application

To illustrate the performance of the proposed model in a real-world context, we apply it to fine particulate matter (PM) data from the Central Valley region of California, USA. Hasheminassab et al. (2014, Sec. 4) analyzed long-term $PM_{2.5}$ records from multiple monitoring stations in the San Joaquin Valley (i.e., the southern portion of the Central Valley) and identified persistent spatial gradients in particulate concentrations. Their findings indicated that secondary aerosol formation and regional transport processes dominate the $PM_{2.5}$ burden, resulting in markedly higher concentrations in the southern and central subregions compared with the northern area. Such spatial heterogeneity suggests that the underlying spatial dependence structure in this region is anisotropic.

We focus on PM_{10} (Response 1) and $PM_{2.5}$ (Response 2), which exhibit a strong positive correlation. Hourly data were obtained from 21 monitoring stations that measured both pollutants between January 1 and December 31, 2024. Daily means were computed, yielding T=366 observations. The dataset was retrieved from the United States Environmental Protection Agency (2025).

Of the $21 \times 366 = 7686$ potential daily observations for each variable, 10.71% were missing in Response 1 and 1.61% in Response 2. We selected N=18 stations for model fitting and reserved $N^*=3$ additional stations for evaluating interpolation performance. Figure 5 depicts the spatial configuration of these monitoring sites.

The analysis was performed without explanatory covariates (p = 1), considering $\mathbf{W} = \mathbf{I}_1$ and, for $t \in \{1, \dots, 366\}$, $\mathbf{G}_t = \mathbf{I}_1$, $\mathbf{X}_t = \mathbf{1}_N$, and $\mathbf{X}_t^* = \mathbf{1}_{N^*}$. To implement Algorithm 5, we used the observed subvectors $\mathbf{y}_{1,\mathsf{obs}}, \dots, \mathbf{y}_{366,\mathsf{obs}}$ and specified the

Table 7: Interval scores by model for different ungauged sites (\mathfrak{s}_{17} , \mathfrak{s}_{18} , and \mathfrak{s}_{19}), response variables ($i \in \{1,2\}$), sample sizes ($T \in \{100,500\}$), and fractions of missing values ($\gamma \in \{0.15,0.30\}$), resulting from the simulation study. The smallest values are in bold.

Site	i	T	γ	\mathcal{M}_1	\mathcal{M}_2	\mathcal{M}_3	\mathcal{M}_4	
§ 17		100	$0.15 \\ 0.30$	0.0288 0.0296	0.0272 0.0276	$0.0256 \\ 0.0272$	$0.0254 \\ 0.0260$	
	1		0.30	0.0290	0.0270	0.0272	0.0251	
		500	0.13	0.0287 0.0300	0.0275 0.0280	0.0254 0.0270	0.0251 0.0265	
		100	0.15	0.0294	0.0285	0.0250	0.0255	
	2		0.30	0.0316	0.0295	0.0265	0.0262	
		500	0.15	0.0286	0.0276	0.0252	0.0249	
			0.30	0.0300	0.0288	0.0268	0.0260	
		100	$0.15 \\ 0.30$	0.0315 0.0304	0.0307 0.0280	$0.0295 \\ 0.0277$	$0.0281 \\ 0.0256$	
	1		0.15	0.0294	0.0282	0.0259	0.0257	
§ 18		500	0.10	0.0294 0.0316	0.0294	0.0239 0.0279	0.0268	
	-	100	0.15	0.0306	0.0294	0.0283	0.0281	
	2	2		0.30	0.0331	0.0316	0.0315	0.0304
					500	0.15	0.0301	0.0296
			0.30	0.0325	0.0305	0.0294	0.0282	
		100	$0.15 \\ 0.30$	0.0280 0.0296	0.0276 0.0281	$0.0269 \\ 0.0288$	$0.0255 \\ 0.0258$	
	1							
		500	$0.15 \\ 0.30$	0.0285 0.0306	0.0277	0.0269 0.0280	$0.0263 \\ 0.0264$	
$\mathbf{\tilde{s}}_{19}$					0.0292			
		100	0.15	0.0278	0.0270	0.0277	0.0261	
	2		0.30	0.0293	0.0271	0.0299	0.0270	
		500	0.15	0.0289	0.0282	0.0268	0.0259	
			0.30	0.0309	0.0294	0.0279	0.0264	

following hyperparameters: $a_V = 0.001, \ b_V = 0.001, \ a_{\Sigma} = 0.001, \ \mathbf{b}_{\Sigma} = 0.001 \mathbf{I}_2, \ \mathbf{M}_0 = \mathbf{0}_{1 \times 2}, \ \mathbf{C}_0 = \mathbf{I}_1, \ \boldsymbol{\sigma}_d^2 = 0.4 \cdot \mathrm{diag} \{ \hat{\sigma}_{\mathrm{lon}}^2, \hat{\sigma}_{\mathrm{lat}}^2 \}, \ \mathrm{and} \ \psi = 10.$

Algorithm 5 was executed for 50,000 iterations to sample from the posterior distribution under Model \mathcal{M}_4 , with convergence achieved after approximately $J \approx 25,000$ iterations. The same configuration was employed for the competing models \mathcal{M}_1 , \mathcal{M}_2 , and \mathcal{M}_3 . To mitigate autocorrelation in the Markov chains, we retained every 25th iteration after burn-in, resulting in K = 1000 posterior samples $(j_1 = 25,001, j_2 = 25,026,\ldots,j_{1000} = 49,976)$.

Table 8 summarizes posterior estimates of $V\Sigma_{1,1}$, $V\Sigma_{1,2}$, $V\Sigma_{2,2}$, and ϕ for each model. Reported metrics include the posterior mean, the 95% highest posterior density (HPD) interval, and the Geweke diagnostic statistic. In all cases, Geweke statistics fall within (-1.96, 1.96), indicating satisfactory convergence. The isotropic models \mathcal{M}_1

and \mathcal{M}_2 yielded higher posterior means for ϕ , whereas larger values of $V\Sigma_{1,1}$, $V\Sigma_{1,2}$, and $V\Sigma_{2,2}$ were obtained under the anisotropic models \mathcal{M}_3 and \mathcal{M}_4 . These anisotropic models also produced wider 95% HPD intervals for $\beta_{0:T}$, as illustrated in Figure 6. Figure 7 further shows that the deformed maps estimated under \mathcal{M}_3 and \mathcal{M}_4 exhibit substantial similarity.

Table 8: Posterior mean, 95% HPD interval (HPD), and Geweke statistic (GS) for $V\Sigma_{1,1}$, $V\Sigma_{1,2}$, $V\Sigma_{2,2}$, and ϕ by model, from the application.

Parameter	Metric	\mathcal{M}_1	\mathcal{M}_2	\mathcal{M}_3	\mathcal{M}_4
$V\Sigma_{1,1}$	Mean HPD GS	281.6 199.12–374.22 -0.043	246.6 188.23–319.64 0.047	443.7 279.17–617.08 0.149	400.9 262.40–563.22 -0.324
$V\Sigma_{1,2}$	Mean HPD GS	0.0 _ _	$ \begin{array}{r} 35.6 \\ 26.09 - 49.81 \\ 0.107 \end{array} $	0.0 _ _	77.3 48.32–112.67 -0.090
$V\Sigma_{2,2}$	Mean HPD GS	$ \begin{array}{r} 33.1 \\ 23.87 - 45.00 \\ 0.672 \end{array} $	29.0 21.28–37.97 0.543	58.9 $38.36-85.18$ 0.650	57.0 35.65–82.02 0.235
ϕ	Mean HPD GS	0.917 $0.6272-1.2681$ -0.687	$\begin{array}{c} 1.106 \\ 0.7566 - 1.5157 \\ -0.501 \end{array}$	0.176 $0.1033-0.2478$ -1.064	0.175 0.0998–0.2441 -1.026

Table 9 presents the model comparison criteria. According to the DIC, model \mathcal{M}_4 provides the best fit to the data. The lowest PMSE value is also associated with \mathcal{M}_4 , indicating superior interpolation accuracy. Based on the interval score (IS), \mathcal{M}_4 performs best for PM₁₀ (Response 1), whereas \mathcal{M}_3 tends to perform slightly better for PM_{2.5} (Response 2). Figure 8 illustrates that, for Response 1 at the ungauged site \mathbf{g}_{20} , model \mathcal{M}_4 yields interpolations closer to the observed values. Additionally, it exhibits noticeably narrower 95% credibility intervals, which is consistent with the reported results.

Overall, the application confirms that the anisotropic models (\mathcal{M}_3 and \mathcal{M}_4) yield more reliable and accurate interpolations than the isotropic alternatives (\mathcal{M}_1 and \mathcal{M}_2).

8 Conclusions

In this paper, we developed a Bayesian spatiotemporal model to jointly analyze two or more response variables measured at fixed spatial locations and discrete, equally spaced time points. The main contribution lies in relaxing the assumption of spatial isotropy by introducing a spatial deformation component within a matrix-variate dynamic modeling framework. The model also accommodates incomplete response matrices under the assumption that missing values are Missing Completely at Random (MCAR) (Little and Rubin 2019, Sec. 1.3).

Table 9: Model comparison metrics (DIC, PMSE, and interval scores) for ungauged sites $(\mathfrak{s}_{19}, \mathfrak{s}_{20}, \mathfrak{s}_{21})$ and response variables $(i \in \{1, 2\})$ from the application.

Metric	Site	i	\mathcal{M}_1	\mathcal{M}_2	\mathcal{M}_3	\mathcal{M}_4
DIC PMSE	_ _	- -	$81675.5 \\ 27.2789$	80347.0 26.0028	$76579.9 \\ 25.3166$	$74882.6 \\ 22.9888$
	S 19	1 2	$0.83725 \\ 0.31413$	$0.81240 \\ 0.30915$	$\begin{array}{c} 0.72242 \\ 0.25200 \end{array}$	$\begin{array}{c} 0.72145 \\ 0.25269 \end{array}$
IS	S 20	1 2	$\begin{array}{c} 1.09535 \\ 0.27022 \end{array}$	$\begin{array}{c} 1.03954 \\ 0.26971 \end{array}$	$0.81070 \\ 0.25684$	$0.74511 \\ 0.25682$
	S 21	$\frac{1}{2}$	1.13926 0.28410	$\begin{array}{c} 1.12673 \\ 0.28160 \end{array}$	$\begin{array}{c} 1.03927 \\ 0.25036 \end{array}$	$\begin{array}{c} 1.02768 \\ 0.25158 \end{array}$

Our main finding is that incorporating spatial deformation substantially improves interpolation accuracy in settings with matrix-variate responses. However, we also observed that small sample sizes and large proportions of missing data may adversely affect parameter estimation quality.

In the empirical application discussed in Section 7, the proposed model provided the best interpolation performance, particularly for the first response variable. We believe this result stems from the use of a common deformation for both response variables. Therefore, a promising future direction would be to allow each response variable to possess its own spatial dependence structure.

Other natural extensions of this work include relaxing the Gaussianity assumption, exploring alternative approaches to handle anisotropy and non-MCAR missingness mechanisms, and implementing more efficient Bayesian inference methods such as Hamiltonian Monte Carlo or variational inference techniques.

Acknowledgments

This article is based on the D.Sc. thesis in Statistics of the first author (Bulhões 2024), supervised by the second and third authors. The first author acknowledges financial support from the Coordenação de Aperfeiçoamento de Pessoal de Nível Superior (CAPES), Brazil, during his doctoral studies at the Federal University of Rio de Janeiro (UFRJ). His current research is supported by the Universidade Federal da Bahia (UFBA), Brazil (Edital PRPPG 010/2024 – Programa de Apoio a Jovens Professores(as)/Pesquisadores(as) Doutores(as) – JOVEMPESQ 2024).

The second and third authors acknowledge financial support from the Conselho Nacional de Desenvolvimento Científico e Tecnológico (CNPq), Brazil, through productivity research grants (Bolsas de Produtividade em Pesquisa).

Statements and Declarations

Funding. This work was supported by the Coordenação de Aperfeiçoamento de Pessoal de Nível Superior (CAPES), Brazil; by the Universidade Federal da Bahia (UFBA), Brazil (Edital PRPPG 010/2024 – JOVEMPESQ 2024); and by the Conselho Nacional de Desenvolvimento Científico e Tecnológico (CNPq), Brazil, through productivity research grants awarded to the second and third authors.

Competing interests. The authors declare that they have no competing interests.

Data availability. The essential materials needed to reproduce the Bayesian analyses are provided as Supplementary Material. Specifically, we make available: (i) the Python code used to implement Algorithms 5 and 6 in the simulation study discussed in Section 6 (Simulation.py); (ii) the Python code used to implement the same algorithms in the real-data application presented in Section 7 (Application.py); (iii) the dataset used in the application (DS_CentralValley.txt); and (iv) the file containing the spatial coordinates of the monitoring stations used in the application, which are depicted in Figure 5 (Stations_CentralValley.txt). All Python scripts were executed using Python 3.8 (van Rossum and Drake 2011).

Algorithm 5 implements a data-augmentation MCMC scheme that generates posterior samples of all model parameters as well as posterior draws of the imputed missing values. Algorithm 6 implements the Monte Carlo approximation of the posterior predictive distribution of the interpolated response matrices. The resulting MCMC draws (which are very large text files and therefore not distributed) can be fully reproduced using the provided scripts. The diagnostic and summarization steps used in the paper were carried out in R (R Core Team 2025), but these steps do not alter the posterior output and can be replicated directly from the reproduced samples.

References

- Bruno, F., Guttorp, P., Sampson, P.D., Cocchi, D.: A simple non-separable, non-stationary spatiotemporal model for ozone. Environmental and Ecological Statistics 16(4), 515–529 (2009) https://doi.org/10.1007/s10651-008-0094-8
- Bulhões, R.S.: Spatial deformation in a Bayesian spatiotemporal model for matrixvariate responses. Unpublished D.Sc. thesis, Federal University of Rio de Janeiro, Rio de Janeiro, Brazil (2024)
- Chib, S., Greenberg, E.: Hierarchical analysis of sur models with extensions to correlated serial errors and time-varying parameter models. Journal of Econometrics **68**(2), 339–360 (1995) https://doi.org/10.1016/0304-4076(94)01653-H
- Carter, C.K., Kohn, R.: On Gibbs sampling for state space models. Biometrika 81(3), 541–553 (1994) https://doi.org/10.1093/biomet/81.3.541
- Damian, D., Sampson, P.D., Guttorp, P.: Bayesian estimation of semi-parametric non-stationary spatial covariance structures. Environmetrics $\mathbf{12}(2)$, 161-178 (2001) https://doi.org/10.1002/1099-095X(200103)12:2 $\langle 161::AID-ENV452 \rangle 3.0.CO$;2-G

- Damian, D., Sampson, P.D., Guttorp, P.: Variance modeling for nonstationary spatial processes with temporal replications. Journal of Geophysical Research: Atmospheres 108(D24) (2003) https://doi.org/10.1029/2002JD002864
- Frühwirth-Schnatter, S.: Data augmentation and dynamic linear models. Journal of Time Series Analysis **15**(2), 183–202 (1994) https://doi.org/10.1111/j.1467-9892. 1994.tb00184.x
- Fonseca, T.C.O., Steel, M.F.J.: A general class of nonseparable space–time covariance models. Environmetrics 22(2), 224–242 (2011) https://doi.org/10.1002/env.1047
- Gelman, A., Carlin, J.B., Stern, H.S., Dunson, D.B., Vehtari, A., Rubin, D.B.: Bayesian Data Analysis, 3rd edn. Chapman & Hall/CRC, Boca Raton, FL (2013). https://doi.org/10.1201/b16018
- Gamerman, D., Ippoliti, L., Valentini, P.: A dynamic structural equation approach to estimate the short-term effects of air pollution on human health. Journal of the Royal Statistical Society: Series C (Applied Statistics) 71, 1–31 (2022) https://doi.org/10.1111/rssc.12554
- Gamerman, D., Lopes, H.F.: Markov Chain Monte Carlo: Stochastic Simulation for Bayesian Inference, 2nd edn. Chapman & Hall/CRC, Boca Raton, FL (2006). https://doi.org/10.1201/9781482296426
- Gamerman, D., Quintana, M.S.B., Alves, M.B.: Bayesian modeling for nonstationary spatial point process via spatial deformations. Entropy **26**(8) (2024) https://doi.org/10.3390/e26080678
- Guttorp, P., Schmidt, A.M.: Covariance structure of spatial and spatiotemporal processes. Wiley Interdisciplinary Reviews: Computational Statistics 5(4), 279–287 (2013) https://doi.org/10.1002/wics.1259
- Hasheminassab, S., Daher, N., Saffari, A., Wang, D., Ostro, B.D., Sioutas, C.: Spatial and temporal variability of sources of ambient fine particulate matter (PM $_{2.5}$) in California. Atmospheric Chemistry and Physics $\bf 14(22)$, 12085-12097 (2014) https://doi.org/10.5194/acp-14-12085-2014
- Huerta, G., Sansó, B., Stroud, J.R.: A spatiotemporal model for Mexico City ozone levels. Journal of the Royal Statistical Society: Series C (Applied Statistics) **53**(2), 231–248 (2004) https://doi.org/10.1046/j.1467-9876.2003.05100.x
- Landim, F.M.P.F., Gamerman, D.: Dynamic hierarchical models: An extension to matrix-variate observations. Computational Statistics & Data Analysis **35**(1), 11–42 (2000) https://doi.org/10.1016/S0167-9473(00)00004-9
- Little, R.J.A., Rubin, D.B.: Statistical Analysis with Missing Data, 3rd edn. John Wiley & Sons, Hoboken, NJ (2019). https://doi.org/10.1002/9781119482260

- Mardia, K.V., Goodall, C.R.: Spatial-temporal analysis of multivariate environmental monitoring data. In: Patil, G.P., Rao, C.R. (eds.) Multivariate Environmental Statistics. North-Holland Series in Statistics and Probability, vol. 6, pp. 347–386. North-Holland, Amsterdam (1993). Chap. 16
- Morales, F.E.C., Gamerman, D., Paez, M.S.: State space models with spatial deformation. Environmental and Ecological Statistics **20**(2), 191–214 (2013) https://doi.org/10.1007/s10651-012-0215-2
- Morales, F.E.C., Politis, D.N., Leskow, J., Paez, M.S.: Student's-t process with spatial deformation for spatio-temporal data. Statistical Methods & Applications, 1–28 (2022) https://doi.org/10.1007/s10260-022-00623-8
- Maity, A., Sherman, M.: Testing for spatial isotropy under general designs. Journal of Statistical Planning and Inference **142**(5), 1081–1091 (2012) https://doi.org/10.1016/j.jspi.2011.11.013
- Morales, F.E.C., Vicini, L.: A non-homogeneous Poisson process geostatistical model with spatial deformation. AStA Advances in Statistical Analysis **104**(3), 503–527 (2020) https://doi.org/10.1007/s10182-020-00373-6
- Neal, R.M.: Slice sampling. The Annals of Statistics $\bf 31(3)$, 705-767 (2003) https://doi.org/10.1214/aos/1056562461
- Paez, M.S., Gamerman, D., Landim, F.M.P.F., Gonzales, E.S.: Spatially varying dynamic coefficient models. Journal of Statistical Planning and Inference **138**(4), 1038–1058 (2008) https://doi.org/10.1016/j.jspi.2007.03.060
- Perrin, O., Meiring, W.: Identifiability for non-stationary spatial structure. Journal of Applied Probability **36**(4), 1244–1250 (1999) https://doi.org/10.1239/jap/1032374771
- Quintana, J.M.: Multivariate Bayesian forecasting models. Unpublished Ph.D. thesis, University of Warwick, Coventry, UK (1987)
- R Core Team: R: A Language and Environment for Statistical Computing. R Foundation for Statistical Computing, Vienna, Austria (2025). R Foundation for Statistical Computing. https://www.R-project.org/
- Rostami-Tabar, B., Rendon-Sanchez, J.F.: Forecasting COVID-19 daily cases using phone call data. Applied Soft Computing 100, 106932 (2021) https://doi.org/10.1016/j.asoc.2020.106932
- Sampson, P.D.: Constructions for nonstationary spatial processes. In: Gelfand, A.E., Diggle, P., Guttorp, P., Fuentes, M. (eds.) Handbook of Spatial Statistics, pp. 119–130. Chapman & Hall/CRC, Boca Raton, FL (2010). Chap. 9. https://doi.org/10.1201/9781420072884-c9

- Spiegelhalter, D.J., Best, N.G., Carlin, B.P., Linde, A.: Bayesian measures of model complexity and fit. Journal of the Royal Statistical Society: Series B (Statistical Methodology) 64(4), 583–639 (2002) https://doi.org/10.1111/1467-9868.00353
- Sampson, P.D., Damian, D., Guttorp, P.: Advances in modeling and inference for environmental processes with nonstationary spatial covariance. In: Monestiez, P., Allard, D., Froidevaux, R. (eds.) geoENV III: Geostatistics for Environmental Applications. Quantitative Geology and Geostatistics, vol. 11, pp. 17–32. Springer, Dordrecht, The Netherlands (2001). https://doi.org/10.1007/978-94-010-0810-5_2
- Sampson, P.D., Guttorp, P.: Nonparametric estimation of nonstationary spatial covariance structure. Journal of the American Statistical Association 87(417), 108–119 (1992) https://doi.org/10.1080/01621459.1992.10475181
- Sansó, B., Guenni, L.: Venezuelan rainfall data analysed by using a Bayesian spacetime model. Journal of the Royal Statistical Society: Series C (Applied Statistics) 48(3), 345–362 (1999) https://doi.org/10.1111/1467-9876.00157
- Shen, Y., Gelfand, A.: Exploring geometric anisotropy for point-referenced spatial data. Spatial Statistics **32**, 100370 (2019) https://doi.org/10.1016/j.spasta.2019. 100370
- Schmidt, A.M., Guttorp, P.: Flexible spatial covariance functions. Spatial Statistics 37, 100416 (2020) https://doi.org/10.1016/j.spasta.2020.100416
- Schmidt, A.M., Guttorp, P., O'Hagan, A.: Considering covariates in the covariance structure of spatial processes. Environmetrics **22**(4), 487–500 (2011) https://doi.org/10.1002/env.1101
- Sampson, P.D., Meiring, W.: Nonstationary Spatial Covariance Modeling Through Spatial Deformation. https://www.stat.washington.edu/peter/PASI/PASI_nonstat1_deform.pdf. Talk in the Pan-American Advanced Study Institute on Spatio-Temporal Statistics, Búzios, Brazil (2014)
- Stroud, J., Müller, P., Sansó, B.: Dynamic models for spatio-temporal data. Journal of the Royal Statistical Society: Series B (Statistical Methodology) **63**, 673–689 (2001) https://doi.org/10.1111/1467-9868.00305
- Schmidt, A.M., O'Hagan, A.: Bayesian inference for non-stationary spatial covariance structure via spatial deformations. Journal of the Royal Statistical Society: Series B (Statistical Methodology) **65**(3), 743–758 (2003) https://doi.org/10.1111/1467-9868.00413
- Tsiko, R.G.: Bayesian spatial analysis of childhood diseases in Zimbabwe. BMC Public Health 15(842), 1–24 (2015) https://doi.org/10.1186/s12889-015-2182-7
- United States Environmental Protection Agency: Outdoor Air Quality Data. Accessed:

January 15, 2025 (2025). https://www.epa.gov/outdoor-air-quality-data

van Rossum, G., Drake, F.L.: The Python Language Reference Manual. Network Theory Ltd., Bristol, UK (2011)

West, M., Harrison, J.: Bayesian Forecasting and Dynamic Models, 2nd edn. Springer, New York, NY (1997). https://doi.org/10.1007/b98971

Winkler, R.L.: A decision-theoretic approach to interval estimation. Journal of the American Statistical Association **67**(337), 187–191 (1972) https://doi.org/10.1080/01621459.1972.10481224

Appendix A Proofs

A.1 Full conditional distribution of V

If $V \sim \text{Inverse-Gamma}(a_V, b_V)$, then the full conditional density of V is given by

$$\begin{split} &f(V \mid \mathbf{y}, \boldsymbol{\beta}_{0:T}, \boldsymbol{\phi}, \mathbf{D}, \boldsymbol{\Sigma}) \propto f(V) f(\boldsymbol{\beta}_{0} \mid V, \boldsymbol{\Sigma}) \\ &\times \prod_{t=1}^{T} \left[f(\boldsymbol{\beta}_{t} \mid \boldsymbol{\beta}_{t-1}, V, \boldsymbol{\Sigma}) f(\mathbf{y}_{t} \mid \boldsymbol{\beta}_{t}, V, \boldsymbol{\phi}, \mathbf{D}, \boldsymbol{\Sigma}) \right] \\ &\propto V^{-a_{V}-1} \exp \left\{ -\frac{b_{V}}{V} \right\} \mathbb{1}_{(0,\infty)}(V) \\ &\times V^{-\frac{pq}{2}} \exp \left\{ -\frac{1}{2V} (\boldsymbol{\beta}_{0} - \mathbf{M}_{0})^{\top} [\boldsymbol{\Sigma} \otimes \mathbf{C}_{0}]^{-1} (\boldsymbol{\beta}_{0} - \mathbf{M}_{0}) \right\} \\ &\times V^{-\frac{Tpq}{2}} \exp \left\{ -\frac{1}{2V} \sum_{t=1}^{T} (\boldsymbol{\beta}_{t} - [\mathbf{I}_{q} \otimes \mathbf{G}_{t}] \boldsymbol{\beta}_{t-1})^{\top} [\boldsymbol{\Sigma} \otimes \mathbf{W}]^{-1} (\boldsymbol{\beta}_{t} - [\mathbf{I}_{q} \otimes \mathbf{G}_{t}] \boldsymbol{\beta}_{t-1}) \right\} \\ &\times V^{-\frac{TNq}{2}} \exp \left\{ -\frac{1}{2V} \sum_{t=1}^{T} (\mathbf{y}_{t} - [\mathbf{I}_{q} \otimes \mathbf{X}_{t}] \boldsymbol{\beta}_{t})^{\top} [\boldsymbol{\Sigma} \otimes \mathbf{B}]^{-1} (\mathbf{y}_{t} - [\mathbf{I}_{q} \otimes \mathbf{X}_{t}] \boldsymbol{\beta}_{t}) \right\} \\ &\propto V^{-a'_{V}-1} \exp \left\{ -\frac{b'_{V}}{V} \right\} \mathbb{1}_{(0,\infty)}(V), \end{split}$$

where

$$a'_{V} = a_{V} + \frac{pq}{2} + \frac{Tpq}{2} + \frac{TNq}{2},$$
 (A1)

and

$$b'_{V} = b_{V} + \frac{1}{2} (\mathring{\beta}_{0} - \mathring{\mathbf{M}}_{0})^{\top} [\mathbf{\Sigma} \otimes \mathbf{C}_{0}]^{-1} (\mathring{\beta}_{0} - \mathring{\mathbf{M}}_{0})$$

$$+ \frac{1}{2} \sum_{t=1}^{T} (\mathring{\beta}_{t} - [\mathbf{I}_{q} \otimes \mathbf{G}_{t}] \mathring{\beta}_{t-1})^{\top} [\mathbf{\Sigma} \otimes \mathbf{W}]^{-1} (\mathring{\beta}_{t} - [\mathbf{I}_{q} \otimes \mathbf{G}_{t}] \mathring{\beta}_{t-1})$$

$$+ \frac{1}{2} \sum_{t=1}^{T} (\mathring{\mathbf{y}}_{t} - [\mathbf{I}_{q} \otimes \mathbf{X}_{t}] \mathring{\beta}_{t})^{\top} [\mathbf{\Sigma} \otimes \mathbf{B}]^{-1} (\mathring{\mathbf{y}}_{t} - [\mathbf{I}_{q} \otimes \mathbf{X}_{t}] \mathring{\beta}_{t}),$$
(A2)

which implies that

$$[V \mid \mathbf{Y} = \mathbf{y}, \boldsymbol{\beta}_{0:T}, \boldsymbol{\Sigma}, \phi, \mathbf{D}] \sim \text{Inverse-Gamma}(a'_V, b'_V).$$
 (A3)

A.2 Full conditional distribution of Σ

Recall that the matrix Normal distribution $\mathsf{Normal}_{p \times q}(\mathbf{M}, \mathbf{C}, \Sigma)$ is equivalent to the multivariate Normal distribution $\mathsf{Normal}_{pq}(\mathsf{vec}(\mathbf{M}), \Sigma \otimes \mathbf{C})$. Due to this equivalence, note that the proposed model, described by (2), (3), and (4), can be rewritten as follows:

$$\begin{split} [\mathbf{Y}_t \mid \boldsymbol{\beta}_t, V, \phi, \mathbf{D}, \boldsymbol{\Sigma}] &\sim \mathsf{Normal}_{N \times q}(\mathbf{X}_t \boldsymbol{\beta}_t, V\mathbf{B}, \boldsymbol{\Sigma}), \\ [\boldsymbol{\beta}_t \mid \boldsymbol{\beta}_{t-1}, V, \boldsymbol{\Sigma}] &\sim \mathsf{Normal}_{p \times q}(\mathbf{G}_t \boldsymbol{\beta}_{t-1}, V\mathbf{W}, \boldsymbol{\Sigma}), \\ [\boldsymbol{\beta}_0 \mid V, \boldsymbol{\Sigma}] &\sim \mathsf{Normal}_{p \times q}(\mathbf{M}_0, V\mathbf{C}_0, \boldsymbol{\Sigma}). \end{split}$$

To obtain the full conditional distribution of Σ , we consider this alternative formulation of the proposed model within the posterior density (7) corresponding to $[\theta \mid \underline{Y} = \underline{y}]$.

A.2.1 General case

If $\Sigma \sim \text{Inverse-Wishart}_a(a_{\Sigma}, \mathbf{b}_{\Sigma})$, then the full conditional density of Σ is given by

$$\begin{split} &f(\mathbf{\Sigma} \mid \mathbf{y}, \boldsymbol{\beta}_{0:T}, V, \boldsymbol{\phi}, \mathbf{D}) \propto f(\mathbf{\Sigma}) f(\boldsymbol{\beta}_{0} \mid V, \mathbf{\Sigma}) \\ &\times \prod_{t=1}^{T} \left[f(\boldsymbol{\beta}_{t} \mid \boldsymbol{\beta}_{t-1}, V, \mathbf{\Sigma}) f(\mathbf{y}_{t} \mid \boldsymbol{\beta}_{t}, V, \boldsymbol{\phi}, \mathbf{D}, \mathbf{\Sigma}) \right] \\ &\propto |\mathbf{\Sigma}|^{-\left(q + \frac{a_{\mathbf{\Sigma}}}{2}\right)} \exp\left\{ -\frac{1}{2} \operatorname{tr}[\mathbf{b}_{\mathbf{\Sigma}} \mathbf{\Sigma}^{-1}] \right\} \mathbb{1}_{\operatorname{Sym}^{+}(q)}(\mathbf{\Sigma}) \\ &\times |\mathbf{\Sigma}|^{-\frac{p}{2}} \exp\left\{ -\frac{1}{2} \operatorname{tr}[(\boldsymbol{\beta}_{0} - \mathbf{M}_{0})^{\top}[V\mathbf{C}_{0}]^{-1}(\boldsymbol{\beta}_{0} - \mathbf{M}_{0})\mathbf{\Sigma}^{-1}] \right\} \\ &\times |\mathbf{\Sigma}|^{-\frac{T_{p}}{2}} \exp\left\{ -\frac{1}{2} \sum_{t=1}^{T} \operatorname{tr}[(\boldsymbol{\beta}_{t} - \mathbf{G}_{t}\boldsymbol{\beta}_{t-1})^{\top}[V\mathbf{W}]^{-1}(\boldsymbol{\beta}_{t} - \mathbf{G}_{t}\boldsymbol{\beta}_{t-1})\mathbf{\Sigma}^{-1}] \right\} \\ &\times |\mathbf{\Sigma}|^{-\frac{T_{N}}{2}} \exp\left\{ -\frac{1}{2} \sum_{t=1}^{T} \operatorname{tr}[(\mathbf{y}_{t} - \mathbf{X}_{t}\boldsymbol{\beta}_{t})^{\top}[V\mathbf{B}]^{-1}(\mathbf{y}_{t} - \mathbf{X}_{t}\boldsymbol{\beta}_{t})\mathbf{\Sigma}^{-1}] \right\} \\ &\propto |\mathbf{\Sigma}|^{-\left(q + \frac{a'_{\mathbf{\Sigma}}}{2}\right)} \exp\left\{ -\frac{1}{2} \operatorname{tr}[\mathbf{b}'_{\mathbf{\Sigma}}\mathbf{\Sigma}^{-1}] \right\} \mathbb{1}_{\operatorname{Sym}^{+}(q)}(\mathbf{\Sigma}), \end{split}$$

where

$$a_{\Sigma}' = a_{\Sigma} + p + Tp + TN, \tag{A4}$$

and

$$\mathbf{b}_{\Sigma}' = \mathbf{b}_{\Sigma} + (\boldsymbol{\beta}_{0} - \mathbf{M}_{0})^{\top} [V\mathbf{C}_{0}]^{-1} (\boldsymbol{\beta}_{0} - \mathbf{M}_{0})$$

$$+ \sum_{t=1}^{T} (\boldsymbol{\beta}_{t} - \mathbf{G}_{t} \boldsymbol{\beta}_{t-1})^{\top} [V\mathbf{W}]^{-1} (\boldsymbol{\beta}_{t} - \mathbf{G}_{t} \boldsymbol{\beta}_{t-1})$$

$$+ \sum_{t=1}^{T} (\mathbf{y}_{t} - \mathbf{X}_{t} \boldsymbol{\beta}_{t})^{\top} [V\mathbf{B}]^{-1} (\mathbf{y}_{t} - \mathbf{X}_{t} \boldsymbol{\beta}_{t}),$$
(A5)

which implies that

$$[\Sigma \mid \mathbf{\tilde{Y}} = \mathbf{y}, \boldsymbol{\beta}_{0:T}, V, \phi, \mathbf{D}] \sim \text{Inverse-Wishart}_q(a_{\Sigma}', \mathbf{b}_{\Sigma}').$$
 (A6)

A.2.2 Diagonal case

Suppose $f(\Sigma) = \prod_{i=1}^q f(\Sigma_{i,i})$ and assign $\Sigma_{i,i} \sim \mathsf{Inverse\text{-}Gamma}(a_{\Sigma_{i,i}}, b_{\Sigma_{i,i}})$ for all $i \in \{1, \dots, q\}$. The full conditional density of Σ is given by

$$f(\mathbf{\Sigma} \mid \mathbf{y}, \boldsymbol{\beta}_{0:T}, V, \boldsymbol{\phi}, \mathbf{D}) \propto \left[\prod_{i=1}^{q} f(\Sigma_{i,i}) \right] f(\boldsymbol{\beta}_{0} \mid V, \mathbf{\Sigma})$$

$$\times \prod_{t=1}^{T} \left[f(\boldsymbol{\beta}_{t} \mid \boldsymbol{\beta}_{t-1}, V, \mathbf{\Sigma}) f(\mathbf{y}_{t} \mid \boldsymbol{\beta}_{t}, V, \boldsymbol{\phi}, \mathbf{D}, \mathbf{\Sigma}) \right]$$

$$\propto \left(\prod_{i=1}^{q} \Sigma_{i,i}^{-a_{\Sigma_{i},i}-1} \right) \exp \left\{ -\sum_{i=1}^{q} \frac{b_{\Sigma_{i,i}}}{\Sigma_{i,i}} \right\} \prod_{i=1}^{q} \mathbb{1}_{(0,\infty)}(\Sigma_{i,i})$$

$$\times \left(\prod_{i=1}^{q} \Sigma_{i,i}^{-\frac{p}{2}} \right) \exp \left\{ -\frac{1}{2} \operatorname{tr} \left[\mathbf{\Sigma}^{-1} (\boldsymbol{\beta}_{0} - \mathbf{M}_{0})^{\top} [V\mathbf{C}_{0}]^{-1} (\boldsymbol{\beta}_{0} - \mathbf{M}_{0}) \right] \right\}$$

$$\times \left(\prod_{i=1}^{q} \Sigma_{i,i}^{-\frac{Tp}{2}} \right) \exp \left\{ -\frac{1}{2} \operatorname{tr} \left[\mathbf{\Sigma}^{-1} \sum_{t=1}^{T} (\boldsymbol{\beta}_{t} - \mathbf{G}_{t} \boldsymbol{\beta}_{t-1})^{\top} [V\mathbf{W}]^{-1} (\boldsymbol{\beta}_{t} - \mathbf{G}_{t} \boldsymbol{\beta}_{t-1}) \right] \right\}$$

$$\times \left(\prod_{i=1}^{q} \Sigma_{i,i}^{-\frac{TN}{2}} \right) \exp \left\{ -\frac{1}{2} \operatorname{tr} \left[\mathbf{\Sigma}^{-1} \sum_{t=1}^{T} (\mathbf{y}_{t} - \mathbf{X}_{t} \boldsymbol{\beta}_{t})^{\top} [V\mathbf{B}]^{-1} (\mathbf{y}_{t} - \mathbf{X}_{t} \boldsymbol{\beta}_{t}) \right] \right\}$$

$$\propto \prod_{i=1}^{q} f(\Sigma_{i,i} \mid \mathbf{y}, \boldsymbol{\beta}_{0:T}, V, \boldsymbol{\phi}, \mathbf{D}),$$

where $\Sigma^{-1} = \text{diag}\{\Sigma_{1,1}^{-1}, \dots, \Sigma_{q,q}^{-1}\}$

$$f(\Sigma_{i,i} \mid \mathbf{y}, \mathbf{\beta}_{0:T}, V, \phi, \mathbf{D}) \propto \Sigma_{i,i}^{-(a'_{\Sigma_{i,i}} + 1)} \exp\left\{-\frac{b'_{\Sigma_{i,i}}}{\Sigma_{i,i}}\right\} \mathbb{1}_{(0,\infty)}(\Sigma_{i,i}), \tag{A7}$$

$$a'_{\Sigma_{i,i}} = a_{\Sigma_{i,i}} + \frac{p}{2} + \frac{Tp}{2} + \frac{TN}{2},$$
 (A8)

and

$$b'_{\Sigma_{i,i}} = b_{\Sigma_{i,i}} + \frac{1}{2} (\mathbf{\hat{g}}_{i,0} - \mathbf{\hat{M}}_{i,0})^{\top} [V\mathbf{C}_{0}]^{-1} (\mathbf{\hat{g}}_{i,0} - \mathbf{\hat{M}}_{i,0})$$

$$+ \frac{1}{2} \sum_{t=1}^{T} (\mathbf{\hat{g}}_{i,t} - \mathbf{G}_{t} \mathbf{\hat{g}}_{i,t-1})^{\top} [V\mathbf{W}]^{-1} (\mathbf{\hat{g}}_{i,t} - \mathbf{G}_{t} \mathbf{\hat{g}}_{i,t-1})$$

$$+ \frac{1}{2} \sum_{t=1}^{T} (\mathbf{\hat{y}}_{i,t} - \mathbf{X}_{t} \mathbf{\hat{g}}_{i,t})^{\top} [V\mathbf{B}]^{-1} (\mathbf{\hat{y}}_{i,t} - \mathbf{X}_{t} \mathbf{\hat{g}}_{i,t}),$$
(A9)

which implies that

$$[\Sigma_{i,i} \mid \mathbf{Y} = \mathbf{y}, \boldsymbol{\beta}_{0:T}, V, \phi, \mathbf{D}] \sim \text{Inverse-Gamma}(a'_{\Sigma_{i,i}}, b'_{\Sigma_{i,i}}).$$
 (A10)

Appendix B Algorithms

This section collects the computational procedures used for posterior inference, data augmentation, and interpolation. Algorithm 1 describes a one-step hybrid MCMC update for the parameter vector under the four competing models, while Algorithm 2 presents the corresponding sampling scheme to obtain a posterior sample in the absence of missing data. When responses are missing, Algorithm 3 details the imputation of the unobserved components, and Algorithms 4 and 5 define the resulting

data augmentation MCMC scheme that alternates between imputation and parameter updates. Finally, Algorithm 6 shows how posterior samples are combined to construct a Monte Carlo approximation to the predictive distribution $f(\mathbf{y}_{\mathsf{int}} \mid \mathbf{y}_{\mathsf{obs}})$ used for interpolation at ungauged sites.

Algorithm 1 One-step hybrid MCMC update for θ under model \mathcal{M}_h .

```
Require: Current parameter state \boldsymbol{\theta}^{(j)} = \{ \boldsymbol{\beta}_{0:T}^{(j)}, V^{(j)}, \boldsymbol{\Sigma}^{(j)}, \phi^{(j)}, \mathbf{D}^{(j)} \} \in \boldsymbol{\Theta}, observed
      data \mathbf{y} = \{\mathbf{y}_t\}_{t=1}^T, fixed matrices \mathbf{W}, \{\mathbf{X}_t\}_{t=1}^T and \{\mathbf{G}_t\}_{t=1}^T, the hyperparameters,
      and a chosen model \mathcal{M}_h, h \in \{1, 2, 3, 4\} (see Section 6).
Ensure: Updated state \theta^{(j+1)}.
 1: Sample \beta_{0:T}^{(j+1)} from (8) using the FFBS algorithm, conditional on
      \{V^{(j)}, \mathbf{\Sigma}^{(j)}, \phi^{(j)}, \mathbf{D}^{(j)}, \mathbf{y}\}.
 2: Sample \phi^{(j+1)} from (9) using the Metropolis-Hastings algorithm, conditional on
      \{oldsymbol{eta}_{0:T}^{(j+1)}, V^{(j)}, oldsymbol{\Sigma}^{(j)}, \mathbf{D}^{(j)}, \mathbf{y}\}.
 3: if h \in \{3, 4\} then
           Sample \mathbf{D}^{(j+1)} from (10) using the slice sampler, conditional on
      \{\boldsymbol{\beta}_{0:T}^{(j+1)}, \boldsymbol{\phi}^{(j+1)}, V^{(j)}, \boldsymbol{\Sigma}^{(j)}, \mathbf{y}\}, while keeping two sites anchored.
  5: else
           Set \mathbf{D}^{(j+1)} = \mathbf{S}.
  8: Sample V^{(j+1)} from its full conditional distribution (A3), conditional on
      \{\beta_{0:T}^{(j+1)}, \Sigma^{(j)}, \phi^{(j+1)}, \mathbf{D}^{(j+1)}, \mathbf{y}\}.
 9: if h \in \{2, 4\} then
           Sample \Sigma^{(j+1)} from its full conditional distribution (A6), conditional on
      \{\boldsymbol{\beta}_{0:T}^{(j+1)}, V^{(j+1)}, \phi^{(j+1)}, \mathbf{D}^{(j+1)}, \mathbf{y}\}.
11: else
           for i = 1, ..., q do
Sample \Sigma_{i,i}^{(j+1)} from (A10), conditional on the same quantities.
 12:
 13:
 14:
           Set \Sigma^{(j+1)} = \text{diag}\{\Sigma_{1,1}^{(j+1)}, \dots, \Sigma_{q,q}^{(j+1)}\}.
 15:
16: end if
```

17: **return** $\boldsymbol{\theta}^{(j+1)}$.

Algorithm 2 Hybrid MCMC scheme to obtain a posterior sample from $f(\boldsymbol{\beta}_{0:T}, V, \boldsymbol{\Sigma}, \phi, \mathbf{D} \mid \mathbf{y}).$

Require: Initial state $\boldsymbol{\theta}^{(0)} \in \boldsymbol{\Theta}$, observed data $\boldsymbol{y} = \{\boldsymbol{y}_t\}_{t=1}^T$, fixed matrices \boldsymbol{W} , $\{\mathbf{X}_t\}_{t=1}^T$ and $\{\mathbf{G}_t\}_{t=1}^T$, the hyperparameters, a chosen model \mathcal{M}_h , $h \in \{1, 2, 3, 4\}$ (see Section 6), and an integer K (desired posterior sample size).

Ensure: Posterior sample $\{\boldsymbol{\theta}^{(k)}\}_{k=1}^K$ from $f(\boldsymbol{\beta}_{0:T}, V, \boldsymbol{\Sigma}, \phi, \mathbf{D} \mid \boldsymbol{y})$, obtained after the Markov chain has reached convergence (post-burn-in draws).

Stage 1: burn-in and convergence assessment

- 1: Set $j \leftarrow 0$.
- 2: repeat
- Generate $\boldsymbol{\theta}^{(j+1)}$ using Algorithm 1 with input $\boldsymbol{\theta}^{(j)}$.
- Set $j \leftarrow j + 1$.
- 5: until the convergence diagnostics indicate that the chain has converged.
- Set $\tilde{\boldsymbol{\theta}} \leftarrow \boldsymbol{\theta}^{(j)}$.

Stage 2: posterior sampling after convergence

- 7: Set $k \leftarrow 1$.
- 8: Set $\boldsymbol{\theta}^{(0)} \leftarrow \tilde{\boldsymbol{\theta}}$ and $j \leftarrow 0$.
- while $k \leq K$ do
- Generate $\boldsymbol{\theta}^{(j+1)}$ using Algorithm 1 with input $\boldsymbol{\theta}^{(j)}$. 10:
- 11:
- $\begin{array}{l} \text{Set } j \leftarrow j+1. \\ \text{Set } \pmb{\theta}^{(k)} \leftarrow \pmb{\theta}^{(j)}. \end{array}$ 12:
- Set $k \leftarrow k+1$. \triangleright Optional: thinning can be performed here by running several one-step updates before storing the next draw.
- 14: end while

Algorithm 3 Sampling the missing responses from their full conditional distribution.

Require: Current state $\boldsymbol{\theta}^{(j)} \in \boldsymbol{\Theta}$, observed responses $\boldsymbol{y}_{\mathsf{obs}} = \{\boldsymbol{y}_{t,\mathsf{obs}}\}_{t=1}^T$, index sets $\mathcal{T}_{ ext{missing}}$ and $\mathcal{T}_{ ext{partial}}$, and matrices $\{\mathbf{P}_t, \mathbf{L}_{t, ext{obs}}, \mathbf{L}_{t, ext{mis}}\}_{t=1}^{T}$. **Ensure:** Completed dataset $\mathbf{y}^{(j+1)} = \{\mathbf{y}_{t, ext{obs}}, \mathbf{y}_{t, ext{mis}}^{(j+1)}\}_{t=1}^{T}$. 1: **for** t = 1, ..., T **do** if $t \in \mathcal{T}_{\text{missing}}$ then Sample $\mathbf{y}_{t,\mathsf{mis}}^{(j+1)}$ from the marginal distribution in (15). 3: Set the full response vector $\mathbf{y}_t^{(j+1)} \leftarrow \mathbf{y}_{t.\text{mis}}^{(j+1)}$. 4: else if $t \in \mathcal{T}_{partial}$ then Sample $\mathbf{y}_{t,\text{mis}}^{(j+1)}$ from the conditional distribution in (12). 6: Construct the full vector $\mathbf{y}_t^{(j+1)} = \mathbf{P}_t^{-1} \begin{vmatrix} \mathbf{y}_{t,\text{obs}} \\ \mathbf{y}_{t,\text{mis}}^{(j+1)} \end{vmatrix}$. 7: else Set $\mathbf{y}_{t}^{(j+1)} \leftarrow \mathbf{y}_{t, \mathsf{obs}}$. 8: 9: 10: 11: end for 12: **return** $\mathbf{y}^{(j+1)}$.

Algorithm 4 One-step data augmentation update to sample from $f(V, \Sigma, \beta_{0:T}, \phi, \mathbf{D}, \mathbf{y}_{\mathsf{mis}} | \mathbf{y}_{\mathsf{obs}})$.

Require: Current state $\boldsymbol{\theta}^{(j)} \in \boldsymbol{\Theta}$, the current imputed values for the missing responses $\mathbf{y}_{\mathsf{mis}}^{(j)} \in \mathcal{Y}_{\mathsf{mis}}$, observed data $\mathbf{y}_{\mathsf{obs}}$, fixed matrices \mathbf{W} , $\{\mathbf{X}_t\}_{t=1}^T$ and $\{\mathbf{G}_t\}_{t=1}^T$, a chosen model \mathcal{M}_h , $h \in \{1, 2, 3, 4\}$, and the hyperparameters.

Ensure: Updated parameter state $\theta^{(j+1)}$ and new imputed values for the missing responses $\mathbf{y}_{\mathsf{mis}}^{(j+1)}$.

- 1: **Imputation step:** Apply Algorithm 3 using $\{\boldsymbol{\theta}^{(j)}, \mathbf{y}_{\mathsf{obs}}\}$ to obtain the completed dataset $\mathbf{y}^{(j+1)} = \{\mathbf{y}_{t,\mathsf{obs}}, \mathbf{y}_{t,\mathsf{mis}}^{(j+1)}\}_{t=1}^T$, where $\mathbf{y}_{\mathsf{mis}}^{(j+1)}$ denotes the newly imputed values.
- 2: **Posterior step:** Using the completed data $\mathbf{y}^{(j+1)}$ as if fully observed, apply Algorithm 1 to generate the updated parameter state $\boldsymbol{\theta}^{(j+1)}$.
- 3: **return** $\{\boldsymbol{\theta}^{(j+1)}, \mathbf{y}_{\mathsf{mis}}^{(j+1)}\}.$

Algorithm 5 Data augmentation MCMC scheme to obtain a posterior sample from $f(V, \Sigma, \beta_{0:T}, \phi, \mathbf{D}, \mathbf{y}_{\mathsf{mis}} \mid \mathbf{y}_{\mathsf{obs}}).$

Require: Initial state $\{\boldsymbol{\theta}^{(0)}, \mathbf{y}_{\mathsf{mis}}^{(0)}\}$, observed data $\mathbf{y}_{\mathsf{obs}}$, a chosen model \mathcal{M}_h , the

hyperparameters, and the desired posterior sample size K. **Ensure:** Posterior sample $\left\{\boldsymbol{\theta}^{(k)}, \mathbf{y}_{\mathsf{mis}}^{(k)}\right\}_{k=1}^{K}$ from $f(V, \boldsymbol{\Sigma}, \boldsymbol{\beta}_{0:T}, \phi, \mathbf{D}, \mathbf{y}_{\mathsf{mis}} \mid \mathbf{y}_{\mathsf{obs}})$, obtained after the Markov chain has reached convergence (post-burn-in draws).

Stage 1: burn-in and convergence assessment

```
1: Set j \leftarrow 0.
  2: repeat
                    Generate \{\boldsymbol{\theta}^{(j+1)}, \mathbf{y}_{\mathsf{mis}}^{(j+1)}\} using Algorithm 4 with input \{\boldsymbol{\theta}^{(j)}, \mathbf{y}_{\mathsf{mis}}^{(j)}\}.
  5: until the convergence diagnostics indicate that the chain has converged.
  6: Set \widetilde{\boldsymbol{\theta}} \leftarrow \boldsymbol{\theta}^{(j)} and \widetilde{\mathbf{y}}_{\mathsf{mis}} \leftarrow \mathbf{y}_{\mathsf{mis}}^{(j)}.
Stage 2: posterior sampling after convergence
 7: Set k \leftarrow 1.

8: Set \{\boldsymbol{\theta}^{(0)}, \mathbf{y}_{\mathsf{mis}}^{(0)}\} \leftarrow \{\widetilde{\boldsymbol{\theta}}, \widetilde{\mathbf{y}}_{\mathsf{mis}}\} and j \leftarrow 0.

9: while k \leq K do

10: Generate \{\boldsymbol{\theta}^{(j+1)}, \mathbf{y}_{\mathsf{mis}}^{(j+1)}\} using Algorithm 4 with input \{\boldsymbol{\theta}^{(j)}, \mathbf{y}_{\mathsf{mis}}^{(j)}\}.
10:
```

Set $j \leftarrow j + 1$. Set $\{\boldsymbol{\theta}^{(k)}, \mathbf{y}_{\mathsf{mis}}^{(k)}\} \leftarrow \{\boldsymbol{\theta}^{(j)}, \mathbf{y}_{\mathsf{mis}}^{(j)}\}$. 12: Set $k \leftarrow k+1$. \triangleright Optional: thinning can be performed here by running several one-step updates before storing the next draw.

14: end while

11:

Algorithm 6 Monte Carlo approximation of $f(\mathbf{y}_{int} \mid \mathbf{y}_{obs})$.

Require: Posterior samples $\left\{\boldsymbol{\theta}^{(j_k)},\, \mathbf{y}_{\mathsf{mis}}^{(j_k)}\right\}_{k=1}^K$ obtained from the posterior sampling scheme (Algorithm 5), observed data $\mathbf{y}_{\mathsf{obs}}$, fixed matrices $\{\mathbf{X}_t^*\}_{t=1}^T$, and the hyperparameters.

Ensure: Monte Carlo sample $\{\mathbf{y}_{\mathsf{int}}^{(j_k)}\}_{k=1}^K$ approximating $f(\mathbf{y}_{\mathsf{int}} \mid \mathbf{y}_{\mathsf{obs}})$.

Generate the interpolated deformation $\mathbf{D}^{*(j_k)}$ using the conditional distribution in (17).

```
for t = 1, \ldots, T do
```

Generate the interpolated response $\mathbf{y}_{t}^{*(j_{k})}$ from the conditional distribution in (18).

5: end for
6: Set
$$\mathbf{y}_{\text{int}}^{(j_k)} \leftarrow \left\{\mathbf{y}_t^{*(j_k)}\right\}_{t=1}^T$$
.
7: end for
8: return $\left\{\mathbf{y}_{\text{int}}^{(j_k)}\right\}_{k=1}^K$.

Appendix C Simulation protocol details

This appendix provides the full simulation setup described in Section 6. Data are generated according to the following steps, which detail the construction of the deformation, the generation of latent states and covariates, and the imposition of missing values.

- 1. **Deformation.** Construct $\mathbf{D} = [\mathbf{d}_{1:2} \ \mathbf{d}_{3:16}]$ and $\mathbf{D}^* = [\mathbf{d}_{17} \ \mathbf{d}_{18} \ \mathbf{d}_{19}]$:
 - (a) Fix the two anchors in \mathcal{D} : $\mathbf{d}_{1:2} = \mathbf{g}_{1:2}$ (i.e., $d(\mathbf{g}_1) = \mathbf{g}_1$ and $d(\mathbf{g}_2) = \mathbf{g}_2$), with $\mathbf{S} = [\mathbf{g}_{1:2} \ \mathbf{g}_{3:16}]$.
- (b) For $n \in \{3, ..., 19\}$, set $\mathbf{d}_n = d(\mathbf{s}_n) = \mathbf{\Lambda} \mathbf{s}_n$, inducing geometric anisotropy via $\mathbf{\Lambda}^{\top} \mathbf{\Lambda} = \mathbf{A}$.

The resulting deformation (Figure 3a) shows axis stretching and a 45° rotation at non-anchor locations.

2. Latent states and covariance. Set the true parameters $V=0.6,\,\phi=0.4,\,\mathrm{and}$

$$\Sigma = \begin{bmatrix} 1.00 & 0.85 \\ 0.85 & 1.00 \end{bmatrix}$$
.

With $C_{0,\text{sim}} = 0.1I_2$, draw $\boldsymbol{\beta}_0 \sim \mathsf{Normal}_{2\times 2}(\mathbf{0}_{2\times 2}, VC_{0,\text{sim}}, \boldsymbol{\Sigma})$. Construct the block matrix

$$\mathbf{B}^{\mathrm{aug}} = \begin{bmatrix} \mathbf{B} & \mathbf{B}_{\mathrm{g,u}} \\ \mathbf{B}_{\mathrm{u,g}} & \mathbf{B}^* \end{bmatrix}$$

of dimension 19 × 19, where \mathbf{B} (16 × 16), $\mathbf{B}_{g,u}$ (16 × 3), $\mathbf{B}_{u,g}$ (3 × 16), and \mathbf{B}^* (3 × 3) have generic element

$$B_{n,n'}^{\operatorname{aug}} = \exp\{-\phi \|d(\mathbf{s}_n) - d(\mathbf{s}_{n'})\|\}.$$

- 3. **Time evolution, covariates, and responses.** For each combination (T, γ) with $T \in \{100, 500\}$ and missing fraction $\gamma \in \{0.15, 0.30\}$, iterate for t = 1, ..., T:
 - (a) Draw $\boldsymbol{\beta}_t \sim \mathsf{Normal}_{2\times 2}(\mathbf{G}_t\boldsymbol{\beta}_{t-1},V\mathbf{W}_{\mathrm{sim}},\boldsymbol{\Sigma})$, where $\mathbf{G}_t = \mathbf{I}_2$ and $\mathbf{W}_{\mathrm{sim}} = \frac{0.2}{T}\mathbf{C}_{0,\mathrm{sim}}$.
 - (b) Generate covariate matrices

$$\mathbf{X}_{t} = \begin{bmatrix} 1 & \cdots & 1 \\ U_{1,t} & \cdots & U_{16,t} \end{bmatrix}^{\top} \quad (16 \times 2), \qquad \mathbf{X}_{t}^{*} = \begin{bmatrix} 1 & 1 & 1 \\ U_{17,t} & U_{18,t} & U_{19,t} \end{bmatrix}^{\top} \quad (3 \times 2),$$

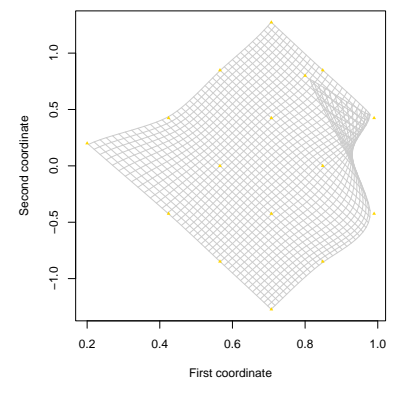
with $U_{1,t}, \ldots, U_{19,t} \sim \mathsf{Uniform}(0,1)$ independently.

(c) Jointly draw

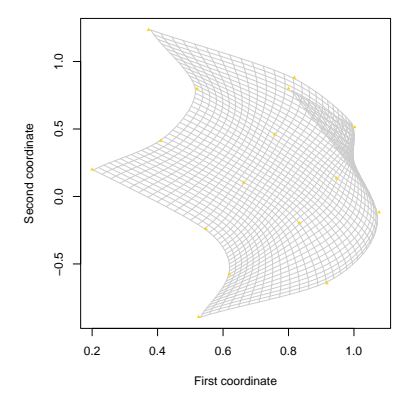
$$\begin{bmatrix} \mathbf{y}_t \\ \mathbf{y}_t^* \end{bmatrix} \sim \mathsf{Normal}_{19 \times 2} \Bigg(\begin{bmatrix} \mathbf{X}_t \\ \mathbf{X}_t^* \end{bmatrix} \boldsymbol{\beta}_t, V\mathbf{B}^{\mathrm{aug}}, \boldsymbol{\Sigma} \Bigg) \,.$$

- (d) Impose missingness: for each response $i \in \{1, \ldots, q\}$, randomly select $\Gamma = \lfloor \gamma N \rfloor$ indices from $\{1, \ldots, N\}$ (without replacement), say n_1, \ldots, n_{Γ} , and set $Y_{n_1, i, t} = \cdots = Y_{n_{\Gamma}, i, t} = \text{NA}$.
- (e) Vectorize $\mathbf{y}_t = \text{vec}(\mathbf{y}_t)$ and obtain the observed subvector $\mathbf{y}_{t,\text{obs}} = \mathbf{L}_{t,\text{obs}} \mathbf{P}_t \mathbf{y}_t$.

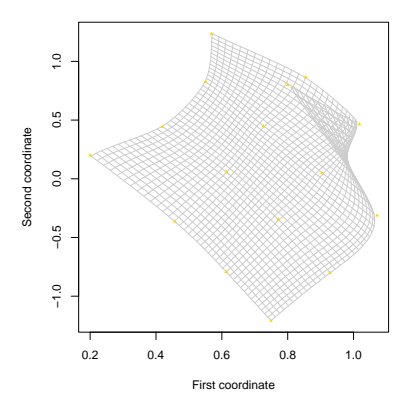
The generated datasets serve as the basis for fitting models \mathcal{M}_1 – \mathcal{M}_4 under the prior and MCMC configurations described in Section 6. These settings ensure reproducibility of the simulation results reported in the main text.



(a) True deformation.



(b) Estimated deformation under Model 3, with T=100 and $\gamma=0.30.$



(c) Estimated deformation under Model 4, with T=500 and $\gamma=0.15.$

Fig. 3: True and estimated deformations under two different scenarios obtained in the simulation study.

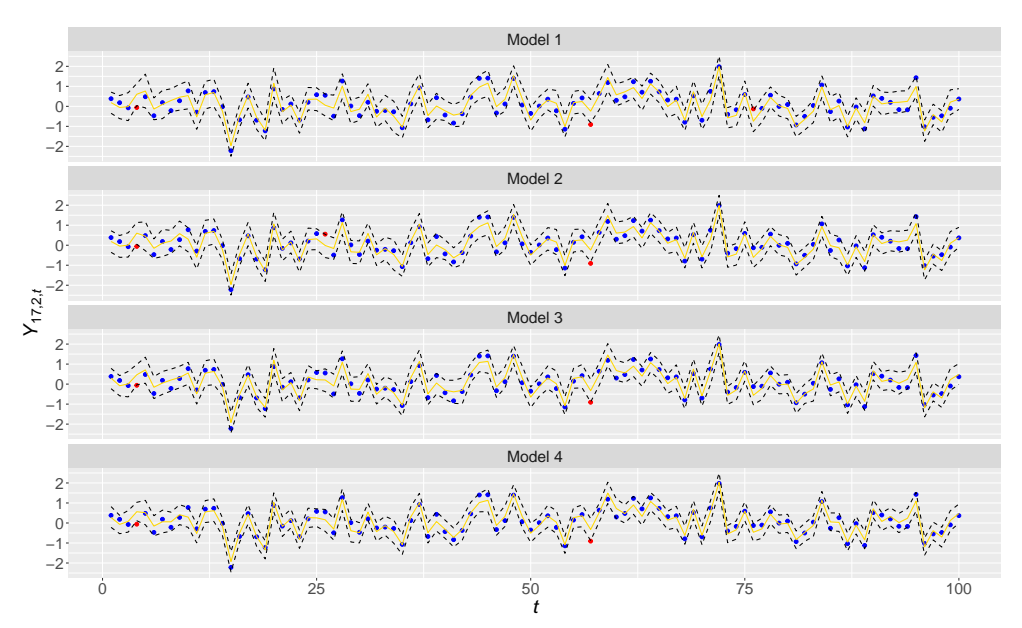


Fig. 4: Line chart of $Y_{n,i,t}$ for n=17, i=1 and $t\in\{1,\ldots,100\}$ by model, resulting from the simulation study $(T=100 \text{ and } \gamma=0.30)$. The 2.5th and 97.5th posterior quantiles are represented by the black dashed lines. Points represent the true values (in blue, if within range; in red, otherwise).

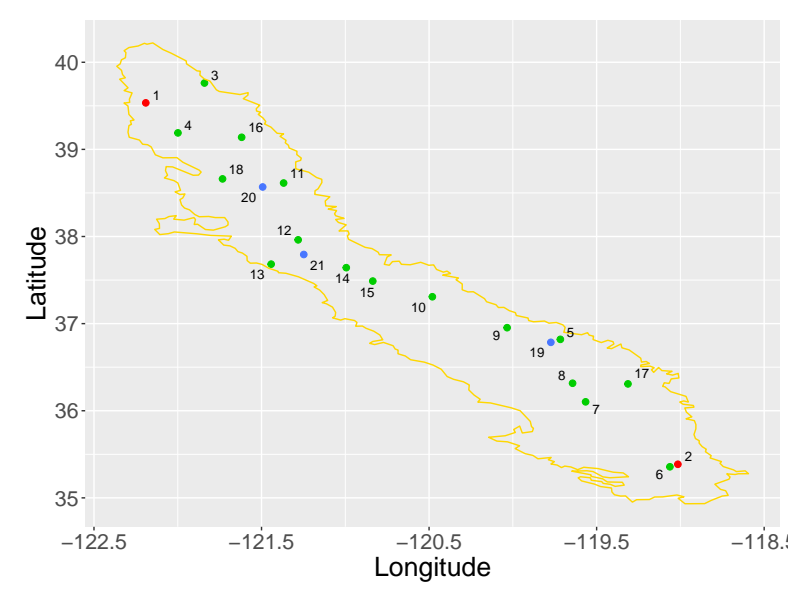


Fig. 5: Central Valley region of California, USA. Anchor sites are shown in red (\S_1 and \S_2), non-anchor gauged sites in green (\S_3, \ldots, \S_{18}), and ungauged sites used for interpolation in blue (\S_{19}, \S_{20} , and \S_{21}).

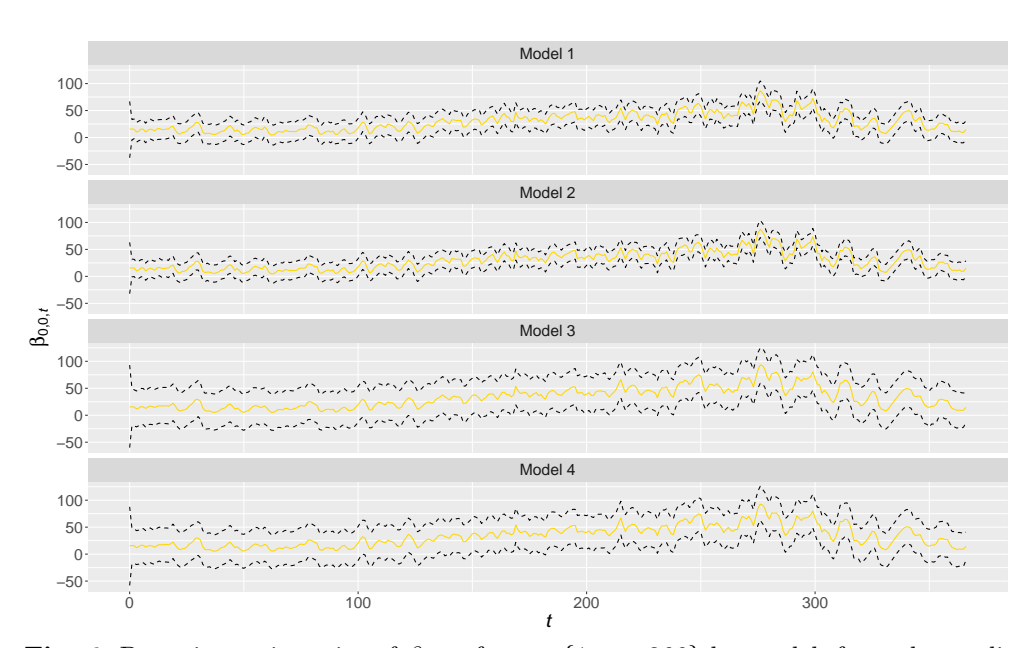
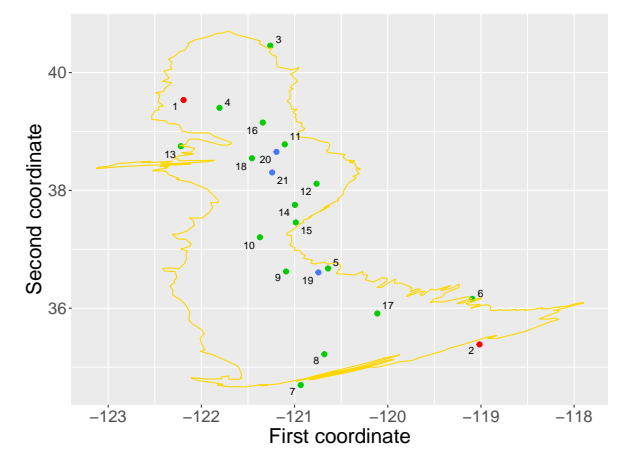
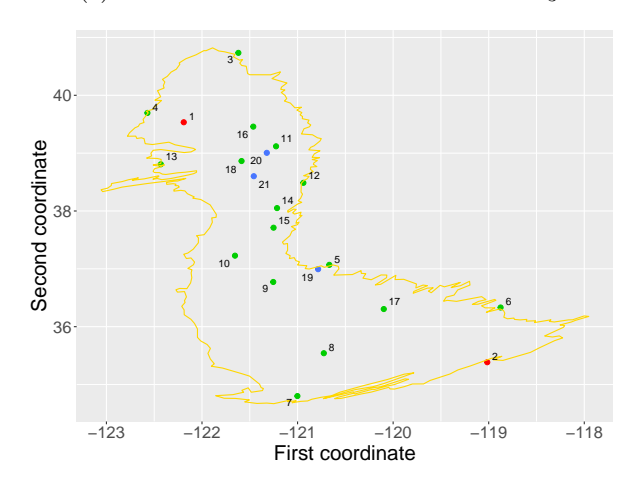


Fig. 6: Posterior trajectories of $\beta_{0,0,t}$ for $t \in \{1,\ldots,366\}$ by model, from the application. The 95% HPD intervals are shown by dashed black lines and posterior means by solid golden lines.



(a) Deformation estimated under Model \mathcal{M}_3 .



(b) Deformation estimated under Model \mathcal{M}_4 .

Fig. 7: Deformations estimated under the anisotropic models \mathcal{M}_3 and \mathcal{M}_4 . Anchor sites are shown in red (\mathbf{g}_1 and \mathbf{g}_2), posterior means of the deformations at non-anchor sites in green ($\mathbf{d}_3, \ldots, \mathbf{d}_{18}$), and posterior means at interpolation sites in blue (\mathbf{d}_{19} , \mathbf{d}_{20} , and \mathbf{d}_{21}).

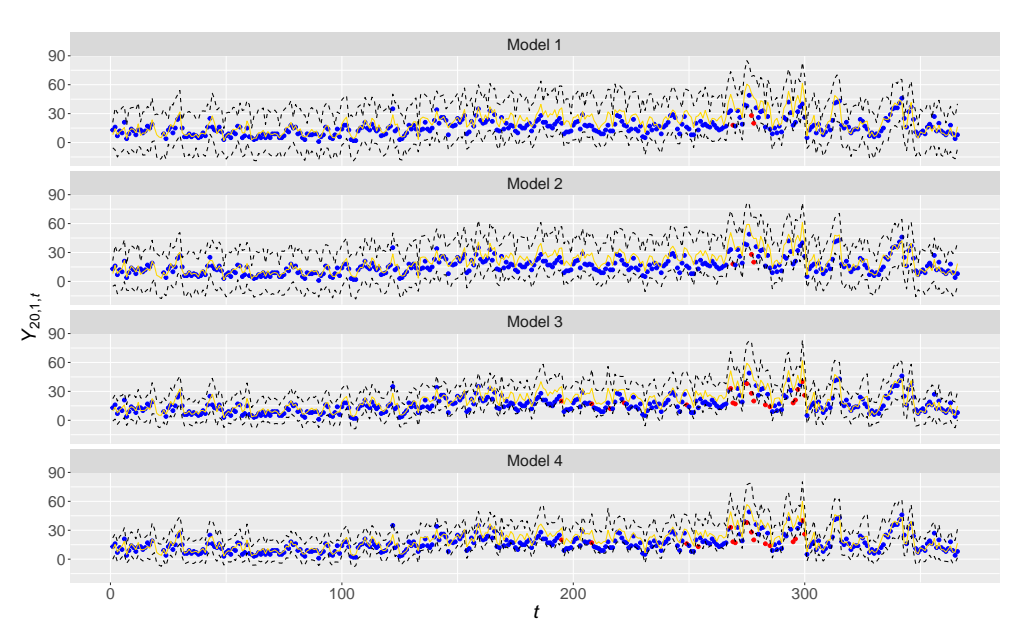


Fig. 8: Posterior trajectories of $Y_{n,i,t}$ for n=20, i=1, and $t\in\{1,\ldots,366\}$ by model, from the application. The 2.5th and 97.5th posterior quantiles are shown by dashed black lines, and observed values by points (blue if within range, red otherwise).